64-8

SPACE POWER AND PROPULSION SECTION

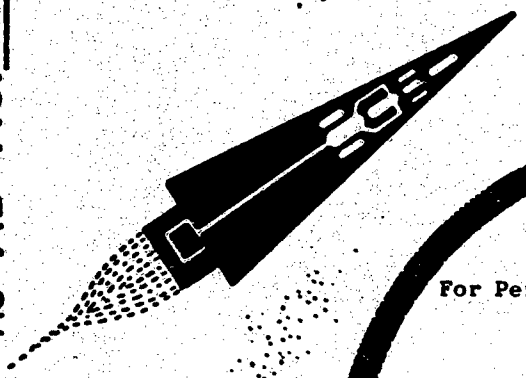

QUARTERLY REPORT #6

For Period Ending October 15, 1963

DYNAMIC SHAFT SEALS IN SPACE

Under Contract #AF33(657)8469

For

Aeronautical Systems Division
Wright Patterson Air Force Base, Ohio

MISSILE and SPACE DIVISION
GENERAL ELECTRIC
CINCINNATI, OHIO

SPACE POWER AND PROPULSION SECTION

QUARTERLY REPORT NO. 6

OCTOBER 15, 1963

DYNAMIC SHAFT SEALS IN SPACE

Under Contract #AF 33(657)-8469

RE-ENTRY SYSTEMS DEPARTMENT
MISSILE AND SPACE DIVISION

GENERAL ELECTRIC COMPANY
CINCINNATI 15, OHIO

TABLE OF CONTENTS

NOMENCLATURE

a	Radius of disk
C_m	Torque coefficient defined by $M = C_m \frac{\rho}{2} \omega^2 a^5$, one side of the disk.
g	Acceleration due to gravity
K	Velocity ratio = $\frac{\beta}{\omega}$
β	Angular velocity of fluid ring
ω	Angular velocity of rotating element
M	Frictional torque
p	Pressure
Re	Reynolds number based on disk radius $Re = \frac{\omega a^2}{\nu}$
s	Axial Distance between disks
u	Absolute tangential velocity component
v	Absolute radial velocity component
V_o	Reference radial velocity near stator
V_o^*	Reference radial velocity near rotor
z	Distance normal to rotor or stator
δ	Rotating disk boundary layer thickness
δ_2	Stationary disk boundary layer thickness
ϵ	Cylindrical wall boundary layer thickness
μ	Dynamic viscosity
ρ	Mass density
τ_o	Boundary shear stress
τ_r	Radial component of shear stress
τ_t	Tangential component of shear stress
ν	Kinematic viscosity

NOMENCLATURE (continued)

r	Radius
r_H	Radius of fluid level on high pressure side of the disk
r_L	Radius of fluid level on low pressure side of the disk
ϕ	$= V_o \vartheta$
x	$x = \frac{a - r}{a}$ or $\frac{b - r}{b}$ submersion ratio
F	Thrust
W	Loss of gas due to absorption by the liquid
C	Molar Concentration
D	Mass diffusivity
T	Temperature

I. SUMMARY

The Space Power and Propulsion Section of the General Electric Company has been under contract to the Aeronautical Systems Division, Wright Patterson Air Force Base, Ohio, since April 15, 1962, for the development of dynamic shaft seals for space applications. The objective of this program is to acquire the techniques for sealing high speed rotating shafts under the operating conditions of high temperature liquid metals and vapors, the near-vacuum environments of space, and to provide long seal life.

A. The contract specifies the following requirements:

1. The fluid to be sealed shall be potassium.
2. The seals shall be operative at fluid temperatures from the melting point of the fluid selected to 1400°F.
3. The pressure on the fluid side of the seal shall be 15 psi and the external pressure shall be 10^{-6} mm Hg.
4. The speed of the rotating shaft shall be a maximum of 36,000 rpm.
5. The seal, or seal combinations, shall be designed for 10,000 hours of maintenance-free life.
6. The working fluid, potassium, shall be used as the seal lubricant.
7. The seal, or seal combinations, shall be capable of maintaining zero leakage - in the technical sense - under all conditions of operation.
8. The seals shall be designed for a 1.0 inch diameter shaft.
9. The seals shall be capable of operating in a zero "g" environment.

B. The seal evaluation shall consist of:

1. Preliminary experiments with water.

2. 100-Hour operational screening test with liquid metal.

3. Thermal-cycling test with liquid metal.

4. 3000-Hour life test with liquid metal.

This report covers progress during the quarter ending October 15, 1963. The main events of this reporting period are:

1. A theoretical investigation of rotating fluid ring seals has been completed. The analysis predicts the performance of plain rotating housing and rotating disk seals.

2. The experimental investigation of the interface instability associated with rotating fluid ring seals continued utilizing the water seal test rig in Building 302. The testing provided additional data concerning the extreme operating range of the DZL seals which were designed to alleviate the interface instability problem. So far, two seal concepts have been developed which suppressed liquid leakage up to speeds of 20,000 RPM.

3. Water seal testing was also performed on the rotating disk-squeeze seal configuration to obtain additional test data for correlating the squeeze seal results with theoretical analysis.

4. The open loop of the water seal rig facility was converted to a close loop so that other fluids such as oil can be evaluated as sealing fluids. Seal testing for the SNAP 8 project using Dow's ET378 oil was initiated. This work was performed under a sub-contract from the General Electric Advanced Technology Laboratory. Both DZL (Dynamic zero leakage) seal configurations which were previously checked out in water were evaluated with

this fluid. The ET 378 has a considerably lower vapor pressure-temperature relationship than water. Therefore attempts have been made to seal atmospheric air against a vacuum of 29 inch Hg utilizing the converted water seal test rig. With the existing seal configurations designed for water operation, vacuum sealing was successfully obtained at speeds above 7000 Rpm. The tests were basically of qualitative nature, however, no liquid fluid leakage due to fluid ring interface instability on the vacuum side could be observed up to the maximum testing speed of 15,000 RPM with the seal configurations designed for the liquid metal test phase. The seal investigations with ET 378 oil continue.

5. Manufacture of the liquid metal seal test facility continued according to the revised schedule. Installation of piping and hardware has been 75% completed.

6. The liquid metal seal test rig manufacture continues. All drawings on the basic test rig including the liquid metal seal configuration have been finalized. Presently process specifications for manufacture are being prepared.

7. All metallurgical data required for the manufacture of the liquid metal seal test rig has been obtained.

II. THEORETICAL INVESTIGATION OF ROTATING FLUID RING SEALS

1. INTRODUCTION

The contact-free dynamic shaft seal has recently become important due to the extreme operating requirements of a space power system. These requirements include high rotational speed, long life, operation in a vacuum, and zero leakage of working fluids. Of the various methods of providing such a seal that have been investigated, one of the most promising is the slinger seal, which consists of a circular disk in a housing. A fluid is introduced into the housing and is thrown to the periphery of the housing by either rotating the disk or the housing. The liquid fluid ring that is formed due to this rotation acts as the seal.

It is the purpose of this report to investigate the flow within the seal and to theoretically develop expressions for the significant seal parameters.

The type of flow within the seal depends upon the seal geometry and the Reynolds number of the rotating element. The different flow regimes that may exist are:

Ia. CLOSE CLEARANCE, LAMINAR FLOW. The boundary layers on the rotor and stator are merged.

Ib. CLOSE CLEARANCES, TURBULENT FLOW. Same as Regime Ia except that the boundary layers are turbulent.

IIa. SEPARATE BOUNDARY LAYERS, LAMINAR FLOW. A core region exists between the boundary layers on the rotor and stator. No change in velocity is expected to occur in this core.

IIb. SEPARATE BOUNDARY LAYERS, TURBULENT FLOW. Same as Regime IIa except that the boundary layers are turbulent.

At this time experiments with slinger seals indicate that only Regime IIb is encountered. Therefore, this analysis applies only to the case of separate boundary layers on the disks and a rotating core fluid between the boundary layers.

The following assumptions are made for the case of separate turbulent boundary layers on the disks and cylindrical wall. Figure 1 is a sketch of the seal and shows the various nomenclature. The fluid outside the boundary layers rotates as a solid body with an angular velocity, $\beta = K\omega$. This velocity is assumed constant over the wetted surface and is in the range $0 < K < 1.0$. All the radial flow occurs within the boundary layers; fluid flows radially outward on the rotating disk in a boundary layer of thickness δ, axially away from the rotating disk in the layer on the cylindrical wall of thickness ϵ, and radially inward on the stationary disk in a layer of thickness γ. The axial pressure gradient in the core fluid is zero, and the pressure in this core is imposed on the boundary layers. The torque of the rotating elements on the fluid is equal to the torque of the fluid on the stationary elements. Radial tip clearance is so small that each side of the disk can be considered separately, and the axial thickness of the disk is considered to be negligible.

This analysis is performed by considering the flow on the rotating disk, the stationary disk, and the cylindrical wall separately. An expression for the frictional moment on each of these elements is developed and then combined for the rotating disk seal and the rotating housing seal.

A friction torque coefficient is then introduced and expressions are developed which allow the determination of this coefficient as a function of disk submersion, axial spacing and Reynolds number. This coefficient is in terms of the friction torque on one side of the disk only.

The thrust that is developed in the seal is also investigated and an expression is derived for this thrust.

Finally, the leakage of a gas due to absorption of the gas by the liquid is studied.

2. DEFINITION OF TERMS

ROTATING DISK SEAL - A seal in which a circular disk rotates in a stationary cylindrical housing.

ROTATING HOUSING SEAL - A seal in which the cylindrical housing rotates and the circular disk is stationary.

SUBMERSION RATIO - A term used to indicate the portion of the disk that is covered by the rotating fluid. It is defined as $x = \frac{a - r}{a}$ where a is the radius of the disk and r is the radius of the fluid surface.

VELOCITY RATIO - The ratio of the angular velocity of the fluid to the angular velocity of the rotating element.

3. THEORETICAL ANALYSIS OF REGIME IIb

The momentum equations for the radial and tangential directions can be written:

STATIONARY DISK

Radial momentum equation

$$\text{(1a)}\quad \frac{\partial}{\partial r}\left(r\int_0^{\vartheta} v^2 dz\right) - \int_0^{\vartheta} u^2 dz = \frac{r}{\rho}\tau_r - r\int_0^{\vartheta}\frac{\partial p}{\partial r}dz$$

Tangential momentum equation

$$\text{(1b)}\quad \frac{\partial}{\partial r}\left(r^2\int_0^{\vartheta} vu\,dz\right) - r^2\beta\frac{\partial}{\partial r}\left(r\int_0^{\vartheta} v\,dz\right) = \frac{r^2}{\rho}\tau_z$$

ROTATING DISK

Radial-momentum equation

$$\text{(2a)}\quad \frac{d}{dr}\left(r\int_0^{\delta} v^2 dz\right) - \int_0^{\delta} u^2 dz = -\frac{r}{\rho}\tau_r - r\int_0^{\delta}\frac{\partial p}{\partial r}dz$$

Tangential-momentum equation

$$\text{(2b)}\quad \frac{d}{dr}\left(r^2\int_0^{\delta} vu\,dz\right) - r^2\beta\frac{d}{dr}\left(r\int_0^{\delta} v\,dz\right) = \frac{r^2}{\rho}\tau_z$$

The exact boundary layer profiles on the disks in this type of flow are not known. Therefore, the boundary layer profiles that have been measured in flow over flat plates have been assumed:

Both disks: $$v = v_0^*\left(\frac{z}{\delta}\right)^{1/7}\left(1-\frac{z}{\delta}\right)$$

(3) Stationary disks: $$u = r\beta\left(\frac{z}{z_0}\right)^{1/7}$$

Rotating disks: $$u = r(\omega-\beta)\left[1-\left(\frac{z}{\delta}\right)^{1/7}\right] + r\beta$$

These profiles allow the calculation of the following integral values, which can be substituted into the momentum equations.

Both disks: $\int_0^\delta v\,dz = \delta V_0^*(.409)$; $\int_0^\delta v^2 dz = \delta V_0^{*2}(.207)$

(4) Stationary disks: $\int_0^\delta u^2 dz = r^2\beta^2\delta(.778)$; $\int_0^\delta vu\,dz = r\beta V_0 2\delta(.3423)$

Rotating disks $\int_0^\delta u^2 dz = r^2\omega^2\delta(.02278) + r^2\omega\beta\delta(.1944) + r^2\beta^2\delta(.778)$

$$\int_0^\delta vu\,dz = r\omega V_0^*\delta(.069) + r\beta V_0^*\delta(.34)$$

For the calculation of $\frac{\partial p}{\partial r}$, the pressure in the boundary layer is assumed to be superimposed on it by the flow outside of the boundary layer. In this flow regime, it is the pressure rise in the core fluid. In the core, there is no radial component of the flow and the velocity of the fluid is given by $U = r\beta$. The pressure gradient can be written as $\frac{\partial p}{\partial r} = \frac{\rho}{r}U^2$, which leads to $\frac{\partial p}{\partial r} = \rho r\beta^2$. This allows the calculation:

$$(5)\quad \int_0^{2\delta}\frac{\partial p}{\partial r}dz = \frac{\partial p}{\partial r}2\delta = \rho\beta^2 r\,2\delta$$

which assumes that the pressure in the core fluid is constant in the axial direction.

The shear stress in the boundary layers is given by:

$$\tau = .022\rho\left[c^2\left(\frac{\nu}{cz}\right)^{1/4}\right]_{z=0}$$ (Reference 2)

which has been experimentally determined for flow in straight ducts. The stress and velocity must be divided into radial and tangential components for use in the momentum equations.

STATIONARY DISK

The shear stress on the stationary disk can be written as:

$$\tau_r = .0225\rho\left(\frac{\nu}{\vartheta}\right)^{1/4}(r\beta)^{3/4}V_0\left(\frac{V_0^2}{r^2\beta^2}+1\right)^{3/8}$$

(6)

$$\tau_\tau = .0225\rho\left(\frac{\nu}{\vartheta}\right)^{1/4}(r\beta)^{3/4}\left(\frac{V_0^2}{r^2\beta^2}+1\right)^{3/8}$$

Substitution of Equations (4), (5), and (6) in the momentum equations (1a) and (1b) yields

$$.207\left(\vartheta V_0^2 r\right)^{I} - .778 r^2\beta^2\vartheta + r^4\beta^4 = .0225\left(\frac{\nu}{\vartheta}\right)^{1/4}V_0 r^{7/4}\beta^{3/4}$$

(7)

$$.34\beta\left(r^3\vartheta V_0\right)^{I} - .409 r^2\beta\left(r\vartheta V_0\right)^{I} = .0225\left(\frac{\nu}{\vartheta}\right)^{1/4} r^{15/4}\beta^{7/4}$$

The term $\frac{V_0^2}{r^2\beta^2}$ is small as compared with 1 and has been neglected. By introducing $\phi = V_0\vartheta$, $x = \frac{b-r}{b}$ and $d = \vartheta^{1/4}$, the fractional exponents of ϑ can be eliminated and Equation (7) assumes the following form.

$$\phi^2 d + 4(1-x)\phi^2 d^I - 2\phi\,\phi^I d(1-x) + 1.073 b^2\beta^2(1-x)^2 d^9 = .1087\beta^{3/4}\nu^{1/4}b^{7/4}\phi\left(1 - 7/4x + \frac{21}{32}x^2 - \frac{21}{384}x^3 + \cdots\right)$$

(8)

$$\phi d + .111(1-x)\phi d = .03676\beta^{3/4}\nu^{1/4}b^{7/4}\left(1 - \frac{7}{4}x + \frac{21}{32}x^2 - \frac{21}{384}x^3 + \cdots\right)$$

The expression $(1 - x)^{7/4}$ has been developed into a series,

$$(1-x)^{7/4} = \left(1 - \frac{7}{4}x + \frac{21}{32}x^2 - \frac{21}{384}x^3 + \cdots\right) \quad (9)$$

The following solutions have been introduced:

$$\phi = x^n\left(C_0 + C_1 x + C_2 x^2 + \cdots\right)$$

(10)

$$d = x^p\left(d_0 + d_1 x + d_2 x^2 + \cdots\right)$$

The method of Variation of Parameters is used to solve these equations. Using this method, N and p have to be selected such that the exponents of x in Equation (8) are different only by integers.. This occurs when

N = 9/10 and P = 1/10.

The coefficients C and d have been determined such that the left hand sides of Equation (13) are identically equal to the right hand sides. A lengthy calculation yields:

$$d = x^{1/10}\left(\frac{\nu}{\beta}\right)^{1/20} b^{3/20}\left(.8554 - 1.063x + .814x^2 + 3.397x^4\right)$$

$$\phi = x^{9/10}\beta^{4/5}\nu^{1/5}b^{8/5}\left(.4254 - 1.894x + 4.47x^2 - 6.945x^3\right) \quad (11)$$

The frictional moment on one side of the disk is given by

$$m = 2\pi\int_0^b \tau_t r^2 dr \quad (12)$$

Combining Equation (6) with Equation (12) gives:

$$m = -2\pi(.0225)\rho b^{19/4}\nu^{1/4}\beta^{7/4}\int_0^1 \frac{(1-x)^{15/4}}{d}dx \quad (13)$$

Since d is a function of x, the integral $\int_0^1 \frac{(1-x)^{15/4}}{d}dx$ must be integrated graphically. Figure 2 is a plot of $\frac{(1-x)}{d}^{15/4}$ vs. x.

Since the curve is asymptotic to the vertical axis, the integration in the range $0 \le x \le .02$ is carried out by assuming $d = x^{1/10}\left(\frac{\nu}{\beta}\right)^{1/20} b^{3/20}(.8554)$ and $(1-x)^{15/4} = 1 - (15/4)x$, which gives

$$m\Big|_0^{.02} = \rho\nu^{1/4}\beta^{7/4}\left(\frac{\beta}{\nu}\right)^{1/20} b^{23/5} 2\pi(.0225)\frac{.0316}{.8554} \quad (14)$$

Integration of the remaining portion of the curve is performed by planimetric methods. The limits of this integration depend upon the wetted portion of the disk and have been taken as X = 1.0, .6, .4, and .2, where X = 1.0 is the case of a completely submerged disk. Table I gives the values of the integral for the various values of X.

TABLE I

X	$\int_{.02}^{X} \frac{(1-x)}{d}^{15/4} dx$	C_1
1.0	.336	.373
.6	.330	.367
.4	.292	.329
.2	.195	.232

The total friction moment for one side of the stationary disk is therefore:

(15) $$M_s = \rho \nu^{1/5} \beta^{9/5} b^{23/5} 2\pi (.0225) \left[.0369 + \int_{.02}^{X} \frac{(1-x)}{d}^{15/4} dx \right]$$

For simplicity, let $C_1 = .0369 + \int_{.02}^{X} \frac{(1-x)}{d}^{15/4} dx$

The values of C_1 are also given in Table I. Equation (15) can then be written as:

(16) $$M_s = 2\pi (.0225) \rho \nu^{1/5} \beta^{9/5} b^{23/5} C_1$$

ROTATING DISK

The substitution of Equations (4), (5) and (6) into Equation (2a) and (2b) gives the momentum equations for the rotating disk:

$$.207\left(r v_o^{*2}\delta\right)^I - .0278 r^2\omega^2\delta - .1944 r^2\omega\beta\delta - .7778 r^2\beta^2\delta + r^2\beta^2\delta = -.0225\left(\frac{\nu}{\delta}\right)^{1/4} v_o^* r^{7/4}(\omega-\beta)^{3/4}\left[\frac{v_o^{*2}}{r^2(\omega-\beta)^2}+1\right]^{3/8} \tag{17}$$

$$.34\omega\left(.2+\frac{\beta}{\omega}\right)\left(r^3 v_o^*\delta\right)^I - .409 r^2\beta\left(r v_o^*\delta\right)^I = .0225\left(\frac{\nu}{\delta}\right)^{1/4} r^{15/4}(\omega-\beta)^{7/4}\left[\frac{v_o^{*2}}{r^2(\omega-\beta)^2}+1\right]^{3/8}$$

(See Footnote)

In these equations γ has been replaced by δ, β by $(\omega-\beta)$, and Vo by Vo*. Dropping the bracket terms with the 3/8 exponents and substituting

$$\delta = \gamma r^{3/5} \quad ; \quad v_o^* = \alpha(\omega-\beta) r \tag{18}$$

into the momentum equation results in:

$$.745\gamma\alpha^2(\omega-\beta)^2 - .0278\omega^2\gamma - .1944\omega\beta\gamma + .222\beta^2\gamma = -.0225\left(\frac{\nu}{\gamma}\right)^{1/4}\alpha(\omega-\beta)^{7/4}$$

(19)

$$\alpha\gamma(\omega-\beta)(.313\omega+.504\beta) = .0225\left(\frac{\nu}{\gamma}\right)^{1/4}(\omega-\beta)^{7/4}$$

Footnote: $(\ )^I$ means derivative with respect to r or z.

These equations can be solved as:

$$\alpha^2 = \frac{1}{\frac{\omega}{\beta}-1}\,\frac{\left(\frac{\omega}{\beta}\right)^2 .0278 + \frac{\omega}{\beta}(.1944) - .222}{\frac{\omega}{\beta}(1.058) - .241} \tag{20}$$

$$\gamma^{1/4} = \left(\frac{\nu}{\beta}\right)^{1/20}\left(\frac{\omega}{\beta}-1\right)^{1/4}\left[\frac{.0225}{(.313\frac{\omega}{\beta}+.504)\alpha}\right]^{1/5}$$

The friction moment on the rotating disk is:

$$M = 2\pi\int_R^a \tau_t\, r^2\, dr \tag{21}$$

and the shear shear stress on the rotating disk is:

$$\tau_t = .0225\,\rho\left(\frac{\nu}{\delta}\right)^{1/4}\gamma^{7/4}(\omega-\beta)^{7/4} \tag{22}$$

Substituting Equation (18) and (22) into Equation (21) gives the moment

$$M_r = 2\pi(.0225)\rho\left(\frac{\nu}{\delta}\right)^{1/4}(\omega-\beta)^{7/4}\int_L^a r^{18/5}\,dr \tag{23}$$

Letting $X = \frac{a-r}{a}$ allows this expression to be dimensionalized and integrated to give the moment on the rotating disk

$$M_r = 2\pi(.0225)\rho\left(\frac{\nu}{\delta}\right)^{1/4}(\omega-\beta)^{7/4}\int_I^0 a^{18/5}(1-x)^{18/5}(-a\,dx) \tag{24}$$

$$M_r = 2\pi\frac{5}{23}(.0225)\rho\left(\frac{\nu}{\gamma}\right)^{1/4}\left(\frac{\omega}{\beta}-1\right)^{7/4}\beta^{7/4}a^{23/5}\left[1-(1-x)^{23/5}\right]$$

CYLINDRICAL WALL

The final portion of the seal that must be considered is the cylindrical wall. The shear stress at the wall is given by:

$$\tau_c = .0225\rho(a\beta)^{7/4}\left(\frac{\nu}{\epsilon}\right)^{1/4} \tag{25}$$

This is the shear stress for turbulent flow through a circular pipe, which is given in Reference 2. Assuming that the boundary layer thickness ϵ is equal to the boundary layer thickness, δ, at the periphery of the rotating disk and utilizing Equation (18) results in

$$\tau_c = .0225\,\rho\left(\frac{\nu}{a}\right)^{1/4} a^{8/5}\,\beta^{7/4} \tag{26}$$

The moment on stationary cylindrical wall is then

$$M = 2\pi a^2 s\,\tau_c = 2\pi(.0225)\rho\left(\frac{\nu}{a}\right)^{1/4} a^{18/5} s\,\beta^{7/4} \tag{27}$$

CALCULATION OF $\frac{\beta}{\omega}$

The torque on the rotating parts of the seal must be equal to the torque on the stationary parts. This requirement allows Equations (16), (24), and (27) to be combined so that the velocity ratio $\frac{\beta}{\omega}$ can be calculated. The two types of seals that are being considered are the rotating disk seal and the rotating housing seal. For analysis purposes, the main difference in the two seals is whether the cylindrical wall is rotating or stationary. Each case is considered separately and the differences can be readily seen.

A. Rotating Disk-Stationary Housing Seal

For the case of the rotating disk seal, the cylindrical wall is stationary and the moment on the stationary parts is the sum of the moments on the staticnary disk and the cylindrical wall, or

$$M_{ST} = 2\pi(.0225)\rho\nu^{1/5}\beta^{9/5}b^{23/5}C_1 + 2\pi(.0225)\rho\left(\frac{\nu}{\gamma}\right)^{1/4}a^{18/5}s\beta^{7/4}$$

$$M_{ST} = 2\pi(.0225)\rho a^{23/5}\left[\nu^{4/20}\beta^{9/5}C_1 + \left(\frac{\nu}{\gamma}\right)^{5/20}\frac{s}{a}\beta^{7/4}\right]$$

However,

$$\gamma^{1/4} = \left(\frac{\nu}{\beta}\right)^{1/20}C_3 \quad ; \quad C_3 = \left(\frac{\omega}{\beta}-1\right)^{1/4}\left[\frac{.0225}{(.313\frac{\omega}{\beta}+.504)a}\right]^{1/5}$$

and

$$\nu^{4/20}\beta^{9/5} = \left(\frac{\nu}{\gamma}\right)^{1/4}\beta^{7/4}C_3$$

Therefore

$$(28)\quad M_{ST} = 2\pi(.0225)\rho a^{23/5}\left(\frac{\nu}{\gamma}\right)^{1/4}\beta^{7/4}\left[C_1C_3 + \frac{s}{a}\right]$$

Equating the moments on the stationary parts and rotating parts gives

$$2\pi(.0225)\rho a^{23/5}\left(\frac{\nu}{\gamma}\right)^{1/4}\beta^{7/4}\left[C_1C_3 + \frac{s}{a}\right] = 2\pi\frac{s}{23}(.0225)\rho a^{23/5}\left(\frac{\nu}{\gamma}\right)^{1/4}\left(\frac{\omega}{\beta}-1\right)^{7/4}\beta^{7/4}\left[1-(1-x)^{23/5}\right]$$

Simplifying and letting $C_2 = 1 - (1 - x)^{23/5}$ yields

$$(29)\quad C_1C_3 + \frac{s}{a} = \frac{s}{23}\left(\frac{\omega}{\beta}-1\right)^{7/4}C_2$$

The value of $\frac{\omega}{\beta}$ that satisfies Equation (29) can be obtained by plotting the left hand side and the right hand side of the equation against the velocity ratio. Their intersection is the value of $\frac{\omega}{\beta}$ for which the moments on the stationary and rotating parts are identical. This has been done in Figure 3 and it can be seen that only one value of $\frac{\omega}{\beta}$ exists for each value of s/a and X.

Figure 4 shows the variation of $K = \frac{\beta}{\omega}$ with $\frac{a - r}{a}$ for various values of s/a. It can be seen that as the amount of submersion decreases, the velocity ratio also decreases. This can be explained by the fact that as the submersion decreases, the area of the cylindrical wall plays a proportionally greater part in retarding the rotation of the fluid.

B. Rotating Housing-stationary Disk Seal

In the rotating housing seal the cylindrical wall is rotating and the moment on this wall must be added to the moment on the rotating disk and their sum equated to the moment on the stationary disk.

Equation (27) must be altered due to the fact that the velocity of the fluid relative to the wall is now $(\omega-\beta)$ instead of β. This leads to:

$$(29) \quad m = 2\pi(.0225)\rho\left(\frac{\nu}{s}\right)^{1/4} a^{18/5} s (\omega-\beta)^{7/4}$$

The total torque on the rotating parts is:

$$(30) \quad m_R = 2\pi(.0225)\rho a^{23/5}\left(\frac{\nu}{s}\right)^{1/4}\left(\frac{\omega}{\beta}-1\right)^{7/4}\beta^{7/4}\left[\frac{s}{23}C_2+\frac{s}{a}\right]$$

Equating (16) and (30) gives:

$$(31) \quad C_1 C_3 = \left(\frac{\omega}{\beta}-1\right)^{7/4}\left[\frac{s}{23}C_2 + \frac{s}{a}\right]$$

The solutions of Equation (31) are shown in Figure 5 and Figure 6 shows the variation of K with $\frac{a - r}{a}$.

Just as the cylindrical wall retarded the flow in the rotating disk seal, it adds a driving surface in the rotating housing seal and results in increases values of K, particularly for small submersions.

TORQUE COEFFICIENT

The coefficient of friction torque is defined by the expression

(32) $$M = C_m \frac{\rho}{2} \omega^2 a^5$$

By equating this defined torque to the torque on the rotating parts (Equations 24 and 30), expressions for C_m are obtained for the rotating disk seal and the rotating housing seal. It is again pointed out that this C_m is for one side of the disk only.

A. Rotating Disk

Equating (32) and (24) yields

$$C_m = \frac{4\pi \frac{5}{23}(.0225) C_2 \left(\frac{\nu}{\omega}\right)^{1/4} \left(\frac{\omega}{\beta} - 1\right)^{7/4} \beta^{7/4}}{a^{2/5} \omega^2}$$

Defining Reynolds number as $Re = \frac{\omega a^2}{\nu}$ and simplifying results in

(33) $$C_m = \frac{.0615 \frac{C_2}{C_3} \left(\frac{\omega}{\beta} - 1\right)^{7/4} \frac{1}{\left(\frac{\omega}{\beta}\right)^{9/5}}}{Re^{1/5}}$$

This equation has been plotted in Figures 7 and 8 to show the variation of C_m with $\frac{a - r}{a}$ and s/a. Since Figure 8 shows that C_m is proportional to $(s/a)^{1/10}$, the following solution was assumed.

(34) $$C_m = \frac{A\left(\frac{s}{a}\right)^{1/10}}{(Re)^{1/5}}$$

A polynomial expression for A in terms of the submersion ratio, X, was obtained by curve fitting and is shown in Figure 9 . This polynomial combined with Equation (34) gives the friction coefficient for one side of a rotating disk in a stationary housing

(35) $$C_m = \frac{(s/a)^{1/10}}{Re^{1/5}}\left(.006 + .168X - .235X^2 + .107X^3\right)$$

B. Rotating Housing

In a manner similar to that used for the rotating disk seal, an expression for the torque coefficient in the rotating housing seal can be written as:

(36) $$C_m = 4\pi(.0225)\left(\frac{s}{23}C_2 + \frac{s}{a}\right)\frac{1}{C_3}\left(\frac{\omega}{\beta} - 1\right)^{7/4}\frac{1}{\left(\frac{\omega}{\beta}\right)^{9/5}}$$

This expression has been plotted in Figures 10 and 11 , which show that C_m varies with approximately the one fifth power of s/a. Therefore, a solution of the form

$$C_m = \frac{A\left(\frac{s}{a}\right)^{1/5}}{R_e^{1/5}}$$

was attempted and the following polynomial for A was obtained.

$$A = .0149 + .1813x - .241x^2 + .106x^3$$

This gives an expression for the friction torque coefficient for one side of a rotating housing seal.

(37) $$C_m = \frac{(s/a)^{1/5}}{(Re)^{1/5}}\left(.0149 + .1813X - .241X^2 + .106X^3\right)$$

To facilitate the use of this expression, the polynomial in X is plotted in Figure 12.

4. THRUST

Another important consideration in this type of seal is the thrust that is developed due to the unequal liquid levels on the two sides of the disk, and to the difference in the angular velocities of the liquids on the opposite sides of the disk.

Consider the configuration shown below, which consists of a rotating and a stationary disk. The radius to the liquid level is denoted by r_o and the static pressure by P_o.

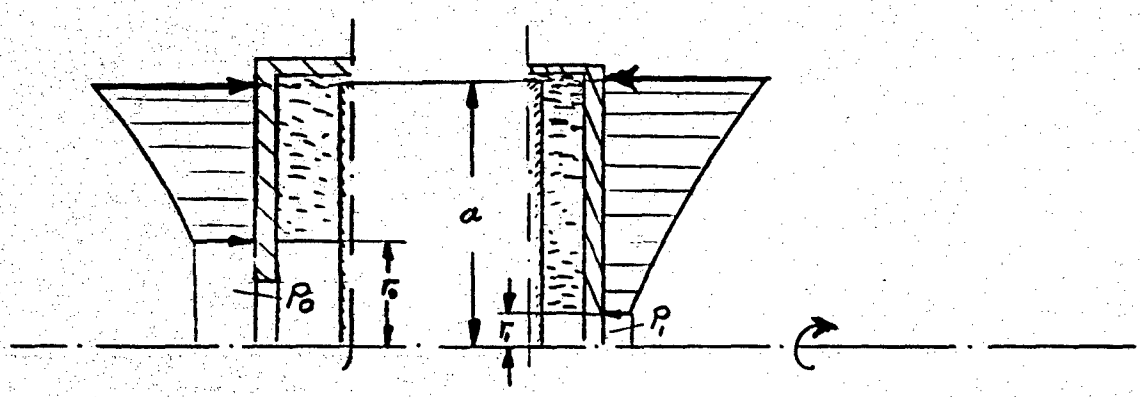

The pressure gradient within the fluid can be written as

(38) $$\frac{dp}{dr} = \rho \beta^2 r$$

Assuming ρ and β constant over the entire core fluid allows the calculation of the hydraulic pressure difference between $r = r_o$ and $r = a$.

(39) $$\Delta p = \frac{\rho}{2} \beta^2 (a^2 - r_o^2)$$

The pressure at any point in the liquid can then be written as:

(40) $$P = P_o + \frac{\rho}{2} \beta^2 (r^2 - r_o^2)$$

The thrust on a small differential of area dA is

(41) $dF = PdA$

Introducing the area $dA = 2\pi r dr$ and using Equation (40) yields

(42) $$dF = \left[P_o + \frac{\rho}{2}\beta^2(r^2 - r_o^2)\right] 2\pi r\, dr$$

Integrating this expression between the limits $r = r_o$ and $r = a$ gives the thrust on the disks due to the hydraulic pressure.

(43) $$F = \pi P_o(a^2 - r_o^2) + \frac{\pi\rho\beta^2}{4}(a^4 - r_o^4) - \frac{\pi\rho\beta^2}{2} r_o^2 (a^2 - r_o^2)$$

Simplifying

(44) $$F = \pi P_o(a^2 - r_o^2) + \frac{\rho}{2}\beta^2(a^2 - r_o^2)\frac{\pi}{2}(a^2 + r_o^2)$$

However, Equation (40) shows that

(45) $$P_T - P_o = \frac{\rho}{2}\beta^2(a^2 - r_o^2)$$

where P_T is the pressure at the tip of the disk.

Combining Equations (41) and (42) gives the thrust due to the hydraulic pressure of the rotating liquid.

(46) $$F = \frac{\pi}{2}(a^2 - r_o^2)(P_T + P_o)$$

In order to apply this equation to a rotating housing seal, consider the following sketch of a typical seal:

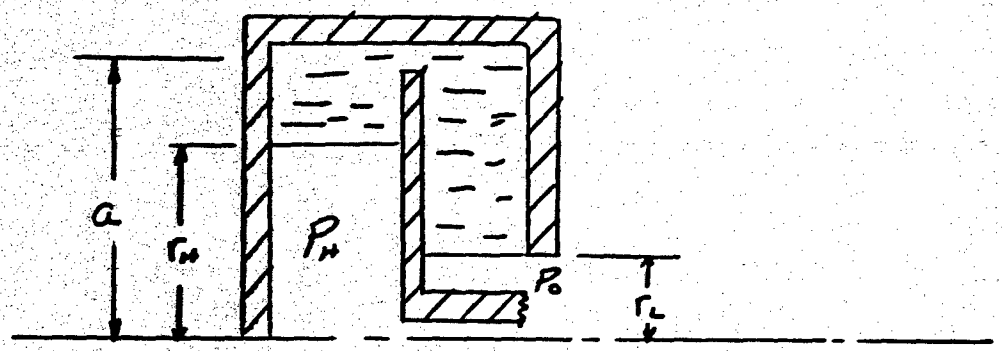

The thrust on the disk is the algebraic sum of the hydraulic and static thrust on both sides of the disk, or

$$F = \Sigma F_{static} + \Sigma F_{hydraulic}$$

Applying Equation (48) to both sides of the disk and assuming that the pressure on the low pressure side is zero, gives the resulting thrust

$$F = \pi r_H^2 P_H + \frac{\pi}{2}(a^2 - r_H^2)(P_H + P_o) - \frac{\pi}{2}(a^2 - r_L^2) P_T$$

Simplifying

$$F = \frac{\pi}{2} P_H (a^2 + r_H^2) + \frac{\pi}{2} P_T (r_L^2 - r_H^2) \quad (47)$$

5. DIFFUSION

The space power systems that use fluid ring seals operate with a limited supply of working fluids. These fluids often consist of gases as well as liquids, which makes the problem of diffusion of the gases into the liquid an important one. Since the fluid seals are often open to the vacuum of space, any gas that is absorbed by the liquid can very easily be lost from the system.

This problem can be approached through the theory of forced-convection mass transfer, as presented in Reference 6. The absorption of a gas by the fluid ring in a seal is analogous to the absorption of a gas by a falling film of liquid. The gas is assumed to be only slightly soluble in the liquid, and to diffuse so slowly that it will not penetrate very far into the liquid. Figure 13 is a sketch of the seal, showing the liquid ring that is assumed to "capture" the gas.

The expression for the diffusion of the gas into the liquid is

$$W = 2\pi r s C \sqrt{\frac{2Du}{\pi^2 r}} \tag{48}$$

where C = molar concentration of the gas at the liquid surface = $\frac{\rho}{M}$

M = molecular weight of the gas

D = Mass diffusivity of the gas in the liquid.

Assuming that the gas behaves as a perfect gas allows the reduction of Equation (48) to the following form:

$$W = 9.1 \times 10^{6} r s C \sqrt{DNK} \tag{49}$$

where

D = cm^2/sec

P = lbs/in^2

r = cm.

s = cm

T = °R

N = Rev./min.

Equation (49) gives the rate at which a gas will be absorbed by the liquid in a slinger seal. The major limitation to this theoretical equation is the determination of an accurate value for the mass diffusivity. Values are not available for any of the fluids that are acceptable for space power systems. The molar concentration of the gas at the liquid interface is also difficult to predict, since it varies with the pressure and temperature, and with the rate at which the liquid vaporizes.

The use of Equation (49) is shown in the following example, which consists of water and air. Assume that air behaves as a perfect gas at sea level condition.

$$C = \frac{\rho}{m} = 3.29 \times 10^{-6} \frac{p}{T} \quad \frac{\text{moles}}{\text{cm}^3}$$

$$W = 870 \frac{s r p}{T} \sqrt{\mathcal{D} N K}$$

$$s = 1\,\text{cm}, \quad r = 2\,\text{cm}, \quad p = 14.7 \frac{\text{lb}}{\text{in}^2}, \quad T = 530^\circ R$$

$$\mathcal{D} = 2 \times 10^{-5} \frac{\text{cm}^2}{\text{sec.}}, \quad N = 24000\,\text{RPM}, \quad K = .5$$

Therefore

$$W = \frac{870(1)(2)(14.7)}{530} \sqrt{(2 \times 10^{-5})(2.4 \times 10^{4})(.5)}$$

$$= 23.7 \quad \text{POUNDS/YEAR}$$

This example shows that the loss of a gas by absorption into the rotating fluid ring of a slinger seal can be appreciable.

6. CONCLUSIONS

Since the only published data on this subject that is available covers the case of a completely submerged rotating disk with a stationary housing, a comparison with existing results must be made on this basis. Figure 14 contains a plot of friction coefficient versus Reynolds number for a completely submerged disk with s/a = .115 (Reference 1), and a plot of C_m verses Reynolds number as taken from Figure 7 for X = 1.0 and s/a = .10. As can be seen the difference between these two results is not too great.

Figure 15 is a plot of the measured values of K as a function of s/a for a completely submerged disk (Reference 1) and a plot of the authors theoretical results taken from Figure 4 . These results also agree very well.

7. RECOMMENDATIONS FOR FURTHER STUDY

1. The velocity profiles that were assumed have been shown (Reference 1) to be accurate for Reynolds numbers less than 10^7. Above this value, little work has been reported. It would, therefore, be beneficial to measure the profiles for Reynolds numbers greater than 10^7, and to modify the theory that is presented here to include these new profiles.

2. Another effect that has been neglected is radial flow within the core. This flow has been observed, but an attempt has not been made to determine the effect of this flow on the torque and velocity ratio.

3. The thrust calculation is based on the assumption that the core fluid rotates as a solid core, and hence the velocity ratio is constant. It has been observed that the effect of radial flow is to retard the rotational velocity of the fluid at small radii. In effect, this makes the velocity ratio a variable with radius, and therefore makes the thrust equation not exactly correct.

III. FLUID DYNAMIC TESTING

1. Investigation of DZL Seals

Fluid dynamic testing of two different DZL (Dynamic Zero Leakage) seals using water as the working fluid continued. Most experiments were made with the wide axial gap DZL seal, because this configuration will be installed on the liquid metal seal test rig. Various axial clearances within the seals and various radial clearances on the close clearance portion of the seal were investigated. This investigation necessarily included the manufacture of additional hardware. This hardware was manufactured from aluminum and plexiglass and therefore did not require long lead times to obtain. The results of the testing of this DZL-seal revealed that the inside axial width of the DZL seal was not critical for acceptable operation of the seals. The radial clearances required within the seal were necessarily small to limit the flow of sealing medium from one chamber of the seal to the other. This limitation on radial clearance, however, is acceptable since the clearances which provided acceptable operation were several times larger than the bearing clearances in a normal turbo machinery design. Both DZL seal configuration with water as a working fluid were successfully operated at speeds up to 20,000 RPM without any loss of liquid sealing fluid due to the interface instability occuring at the inside diameter of the rotating fluid ring on the stationary wall of the seal housing. Sufficient fluid dynamic information on this liquid metal seal configuration have been obtained by now to finalize the seal test rig design.

2. Additional Investigation of the Squeeze Seal

After completion the investigation of the DZL seals the test rig was disassembled and set-up was made for testing miscellaneous squeeze seal configurations. During analysis of test data it became apparent that several operational regimes of the squeeze seal configuration were insufficiently covered by tests. Therefore to complete the squeeze seal test coverage and to allow proper analytical interpretation of the test results, a total of 14 additional tests had to be performed. The testing was done at five speeds up to maximum pressure capability with a constant cooling flow maintained within the seal.

Since the purpose of the testing was to obtain data on the squeeze seal operation and allow the accurate prediction of sealing potential and power requirements it was necessary to test the individual portions of the seal. This meant that the rotating disk and the squeeze portion of the seal were to be separately tested. Therefore, for one half of the tests, the disk was removed from the test rig. Water was then injected within the close clearance squeeze portion of the seal and the leakage from each end was measured. The pressure profile within the squeeze portion of the seal was measured as was the torque requirements. The data from this testing is presently being evaluated.

3. Evaluation of DZL Seals With Oil ET 378

The SPPS Operation was contacted by General Electric's Advanced Technology Operation to evaluate DZL seals using ET 378 organic fluid (Dow Chemical Company, Bis (Phenoxyphenyl) as working medium. This fluid is

intended as bearing and seal fluid of the generator for the NASA sponsored SNAP 8 project and has special outstanding features such as low vapor pressure at elevated temperatures (See Figure 16). The high price and its limited availability forced us to convert the open loop of the water seal rig facility to a close loop (See Figure 17). Both water evaluated DZL seal configurations were tested with this fluid. Basically seal performance concerning liquid leakage due to interface instability was very much the same. After proper operation of the close loop seal facility both DZL seals did not leak liquid organic fluid up to the maximum test speed of 15,000 RPM while the seals were running in normal air atmosphere and were not subjected to a pressure difference. Figure 18 was obtained during interface stability investigation of the narrow gap DZL seal. The photograph shows typical DZL seal operation in air atmosphere without sealing a pressure difference. The seal was photographed while operating at 9,900 RPM. The entire seal disk cavity is filled with rotating ET 378 fluid, however no liquid leakage can be observed leaving the seal through the gap formed between stationary plexiglass sleeve and rotating shaft as seen in the center of the photograph. The leaking fluid which can be seen at the bottom of the seal housing resulted from leaks through bolt holes along the periphery of the stationary plexiglass seal cover. During trials to seal pressurized nitrogen or air, a peculiar phenomena was observed. The organic fluid rapidly dissolved the gas and became foamy. Sealing against pressurized air was therefore not too successful, however, if pressurized gas was introduced on the DZL seal side, liquid leakage due to fluid ring instability did not occur.

After the experience of sealing pressurized gases it was considered quite unlikely that the ET 378 would be a good enough sealing fluid to seal atmospheric air against a vacuum. However, tests were arranged to check both DZL seal configurations under actual vacuum conditions. A typical set-up for vacuum seal testing is shown on Figure 19 . The figure shows the narrow gap DZL seal configuration facing the vacuum chamber together with a rotating disk-squeeze seal arrangement facing the atmospheric air side. Characteristical pressures and temperatures as obtained during testing up to 13,200 RPM are also indicated. After proper seal flow and speed setting (up to 9,000 RPM) the vacuum chamber was evacuated by a mechanical roughening pump down to 28.9 inch Hg. Surprisingly this vacuum in the cnamber during the seal operation could easily be maintained, after a valve in the vacuum extraction line was closed. No leakage due to foaming as observed during the trials to seal pressurized gases could be detected. After improving changes of the seal hardware both DZL seal configurations were capable to sustain the vacuum as produced by the roughening pump between 7000 RPM and the maximum test speed of 15,000 RPM without liquid leakage due to interface instability. The maximum speed was limited by the frictional heat generated in the seal. The results of these simple tests increased considerably the changes of successful application of DZL seals in liquid metal systems.

IV. LIQUID METAL SEAL TEST FACILITIES

1. Seal Rig Facility

The manufacture of the liquid metal seal test facility is proceeding according to the revised schedule. To date components and all the framework of the test facility have been completed. Figure 20 shows the complete assembled facility awaiting a mass spectrometer leak test before it is moved to the actual test area in Building 314.

The installation of the liquid metal seal test facility within Building 314 requires considerable additional installations to the existing building and the facility. Argon supply for the test rigs externally pressurized gas bearings and controll instrumentation for facility and the seal rig have to be installed, before checkout of facility can be initiated.

2. Seal Test Rig

Manufacture of the liquid metal seal test rig continued during this reporting period. Primary manufacturing emphasis was placed on the cold end of the test rig where the test turbine and gas bearing portion of the rig is located. The sundry small parts necessary to mount the test turbine on the rig were manufactured. The hot portion of the seal test rig, the part which operates actually in liquid metal and houses the DZL seal, has been completely designed utilizing the seal information obtained during water and organic fluid seal testing. Presently manufacturing specifications for the individual test rig parts are being prepared and at the end of this month all drawings and the pertinent informations shall be in the hands of the manufacturer. All forgings required for the test rig have been delivered. This includes forgings of the following materials: 316 SS, Rex 49 and Waspalloy.

V. ELECTRON BEAM WELDING OF REX 49 MATERIAL

As discussed in more detail in the last quarterly progress report, Rex 49 was selected as the gas bearing shaft material. Manufacturing considerations made welding of shaft parts desirable, however, insufficient information on welding of Rex 49 forced a detailed investigation of this materials welding capability. Two approaches to the problem were considered to determine the best configuration and requirements for the weld process; first, welding the components before hardening; and second, welding the components in the hardened condition.

The composition of the Rex 49 material is:

%C	Mn	Si	Cr	W	Mo	V	Co
1.10	0.45	0.30	4.25	6.75	3.75	2.0	5.0

The high carbon content and the large amount of carbide forming constituents indicate that fusion welding this material would result in the formation of brittle martensitic structures. Electron beam welding was considered because of the shallow heat affected zones produced by the process and the ability of the electron beam to penetrate to the depth required.

1. Test Outline

1. The dimensions used in the test specimens were taken from the seal shaft design so that the actual weld and heat treat stress conditions could be closely approximated. The assembly was tested with the plug fitting loosely and, in a second instance, with a shrink fit.

The original one-half (1/2) inch thickness of the plug was decreased after an initial weld trial to one-quarter (1/4) inch when this was found to be the maximum depth of penetration of the electron beam welder at 90% of power.

2. The material was in the spherodized annealed condition as received and the first welds made were on specimens in this condition. After welding, the assembly was checked for cracks and promptly tempered. Following the tempering of the weld, the assembly was annealed and heat treated according to recommendations of the Crucible Steel Company Data Sheet on Rex 49; i.e., pre-heat at 1525°F, austenitize fifteen minutes at 2225°F, quench in molten salt at 1100°F, air cool to 150°F and tempered immediately at 1050°F for two hours, then two hours each for two treatments at 1250°F.

   A second series of specimens were hardened as above and tempered at a selected temperature before welding; they were re-tempered at that same temperature immediately following the welding operation. The hardened specimens were evaluated at the following three hardness (or temper) levels; i.e., 1650°F (Specimen D), 1450°F (Specimen E), and 1250°F (Specimen F). As will later be shown, pre-weld hardness did not appear to affect the weldability or resistance to cracking.

3. The machine used in this investigation was a 150 KV, 20 M.A., Hamilton-Zeiss electron beam welder. Activation of the electrom beam was limited by an environmental pressure requirement of no greater than 5×10^{-4} mm of Hg.

Pre-heat and post-heat of the samples was accomplished at 100 KV and 2 M.A. resulting in a temperature of approximately 800°F. Indexing of the beam on the center or the joint was accomplished at 120 KV and 5 M.A. Welding was accomplished at 150 KV and 14 M.A. The specimen was rotated to provide movement of the electron beam around the weld. A circle generator was employed so as to "knit" the joint for optimum fustion of both components. Figure 21 illustrates the desired weld spike and the resultant path traced by the electron beam when the circle generator was employed.

2. Discussion

1. Welding of the Rex 49 material was done first on the as-received, annealed samples. Pre-heat by the electron beam of approximately 800°F was employed on these specimens. Two of the three samples cracked before stress-relieving could be accomplished.

   a. The first specimen (A) was successfully welded and immediately tempered. Following temper of the hardened weld, the assembly was annealed and given the recommended hardening treatment, tempering at 1050°F and 1250°F.

      Figure 22 shows the homogenous condition of the weldment after hoat treatment. The weld is stress cracked near the point of the spike at the weld-base metal interface (not visible in macro).

b. The weld of the second specimen (B) cracked before stress-relief could be accomplished. Following tempering of the first weld, the specimen was "repair welded". The first weld spike was made at 120 KV, 5 M.A., 20 inches/minute, (circle generator was used in all instances at a setting of 14). The repair weld was made at 150 KV, 10 M.A., and other conditions the same as above; the repair resulted in what appeared to be a sound joint. Sectioning of the specimen disclosed a crack in one portion of the joint where the fusion was not complete (Figure 23). Another section of specimen B disclosed no crack; it showed complete fusion of both components (Figure 24).

c. The third annealed sample cracked and was repair welded at 150 KV, 12 M.A. The specimen was sectioned and used to evaluate further weld settings.

2. The second series of electron beam welds was performed on hardened and tempered specimens. The electron beam was indexed on the joint at 120 KV, 2 M.A. and increased to 150 KV, 12 M.A. for welding.

a. Specimen D was hardened and tempered at 1650°F with a resulting hardness of R_c 54. The electron beam was indexed and increased to welding power as indicated above; this resulted in a shift of the beam about .020" radially inward placing the weld spike almost wholly within the plug. Because of the lack of fusion

between plug and cylinder, the plug lifted and tore the ring material as shown in Figure 25 . The amount of weld bond at the tear is shown on Figure 26 . Corrective action was applied to following specimens without complete success. The inability to accurately track along the circumferential weld joint was responsible for lack of complete fusion and cracking.

b. Specimen E was hardened and tempered at 1050°F and 1450°F with a resultant hardness of R_c 55. This specimen was considered to be successfully welded when a cursory examination disclosed no obvious cracks. Later metallographic examination disclosed cracks in the center of the weld; the location of these cracks is shown in Figure 27.

c. Specimen F was hardened and tempered at 1050°F and 1250°F with a resultant hardness of R_c 57. This specimen appeared also to have been successfully welded. The sample was removed from the weld chamber and while being examined for cracks, burst audibly into two pieces (Figure 28). Figures 28 and 29 show that the weld spike was not centered on the joint. Small cracks were found near specimen surface at weld metal-base metal interface.

3. Observations

1. In general, steels having a carbon content in excess of 0.50% require a pre-heat temperature minimum of 500°F and a post-heat

temperature between 1000°F and 1250°F in order to relieve the stresses of the brittle weld metal to prevent cracking.

The beneficial contributions of pre-heat and post-heat could not be accurately determined in these tests on Rex 49 because the electron beam was used as the heat source. The electron beam was diffused to enlarge the heated area but was still concentrated on a small spot on the surface of the specimen. The combined mass of the specimen and fixture removed this heat too rapidly to allow uniform heating of the specimen. Post-heating with the electron beam appeared only to effect the surface of the weld bead.

2. Electron beam welding of this material created a very shallow heat affected zone as can be seen on Figures 30 and 31 . The high hardness of the weld spike can be noted also from the figure.

3. Complete fusion of the joint is necessary because the presence of a notch can (and did) cause a crack to propagate through the brittle weld metal.

4. The electron beam does not appear to be controllable to the degree required at the high power settings which are necessary to penetrate to the full depth of such a joint.

4. Summary

The results of these tests indicate that successful electron beam welding of Rex 49 material cannot be accomplished at the present time with any degree of confidence of electron beam welding of tool steels. In order to advance the present state-of-the-art further investigations into factors such as pre-heat and post-heat temperatures, and electron beam shift characteristics during power level changes are required in order to produce welds with a high degree of confidence.

DYNAMIC SEAL WORK SCHEDULE

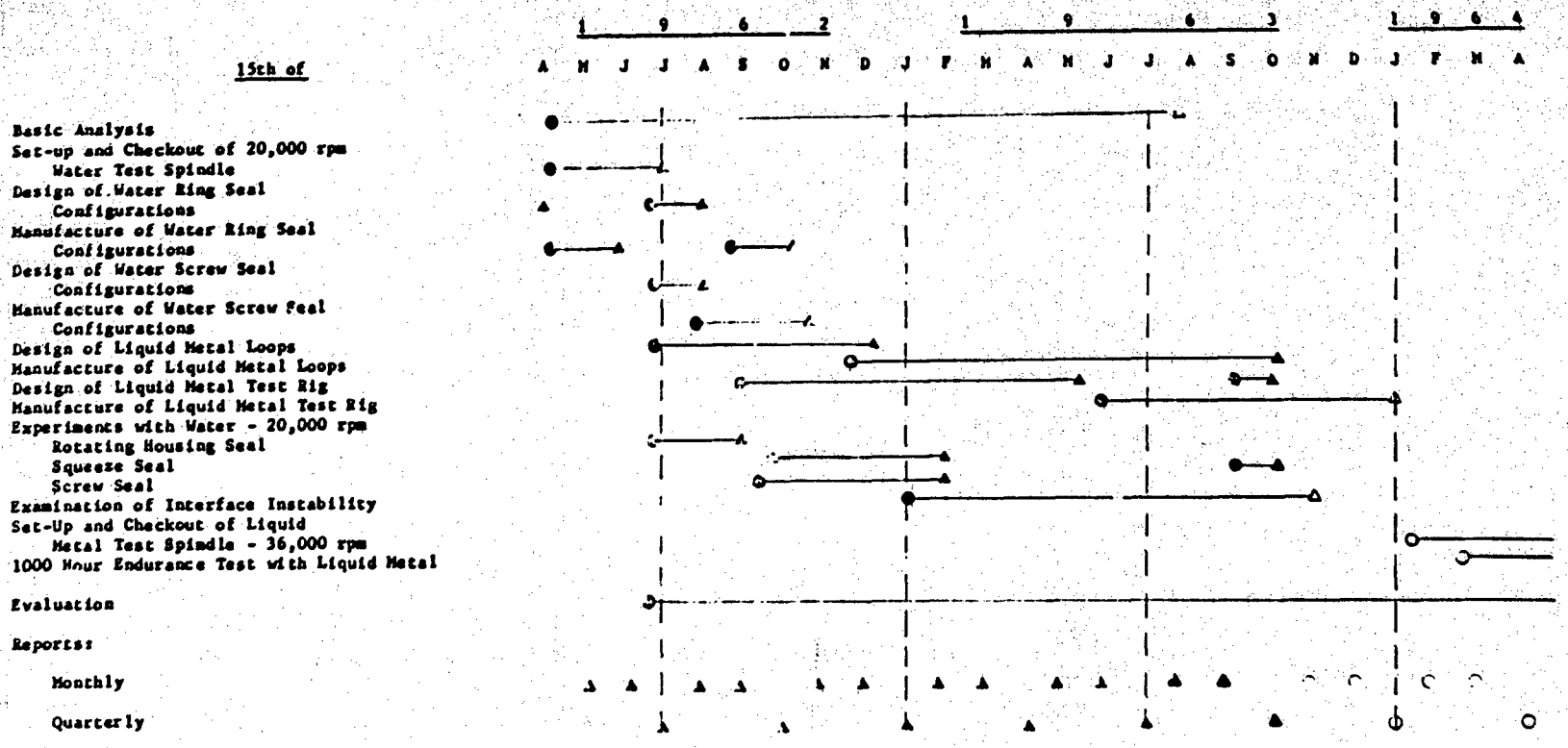

O Start

Δ Complete

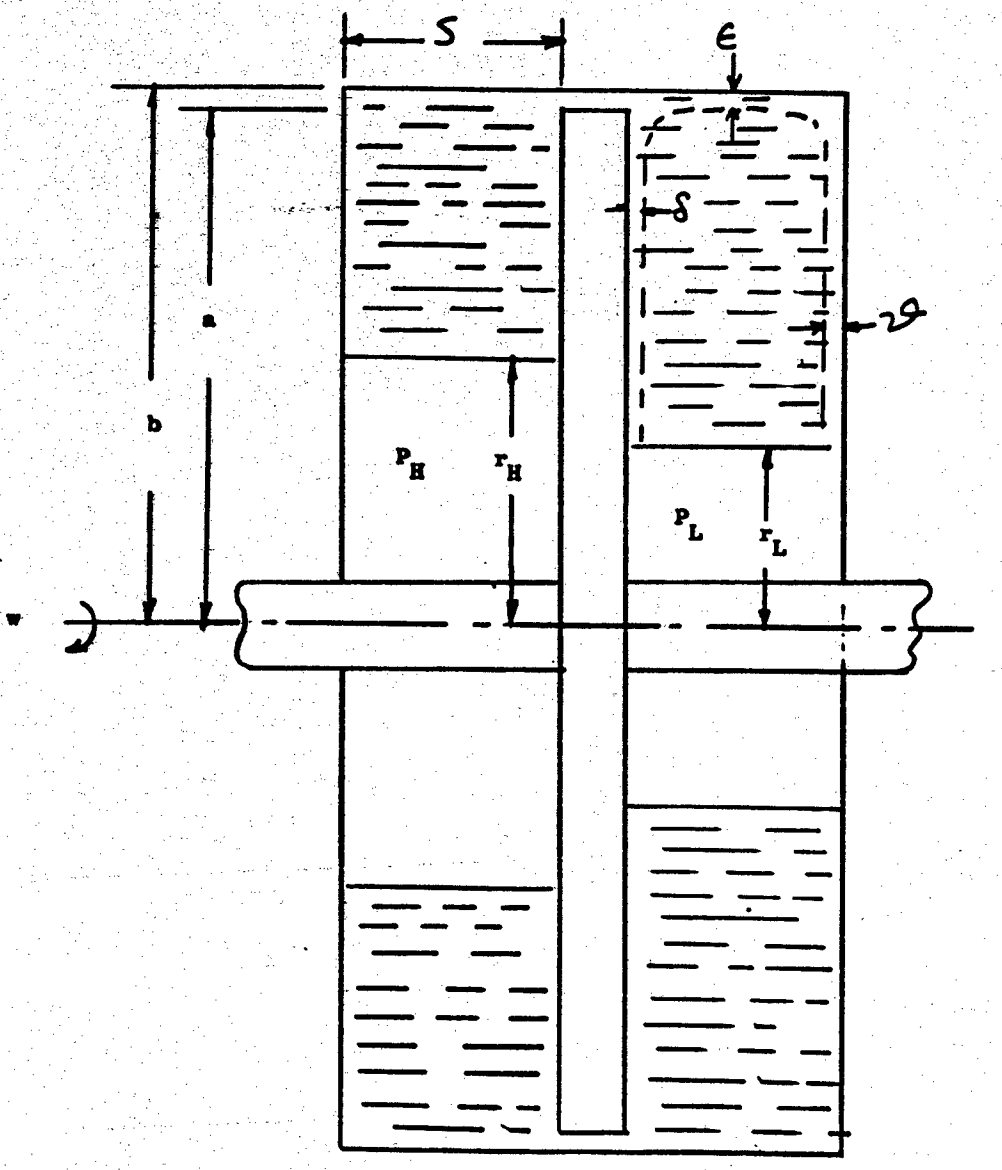

Figure 1. Schematic of a Rotating Disk Seal Configuration.

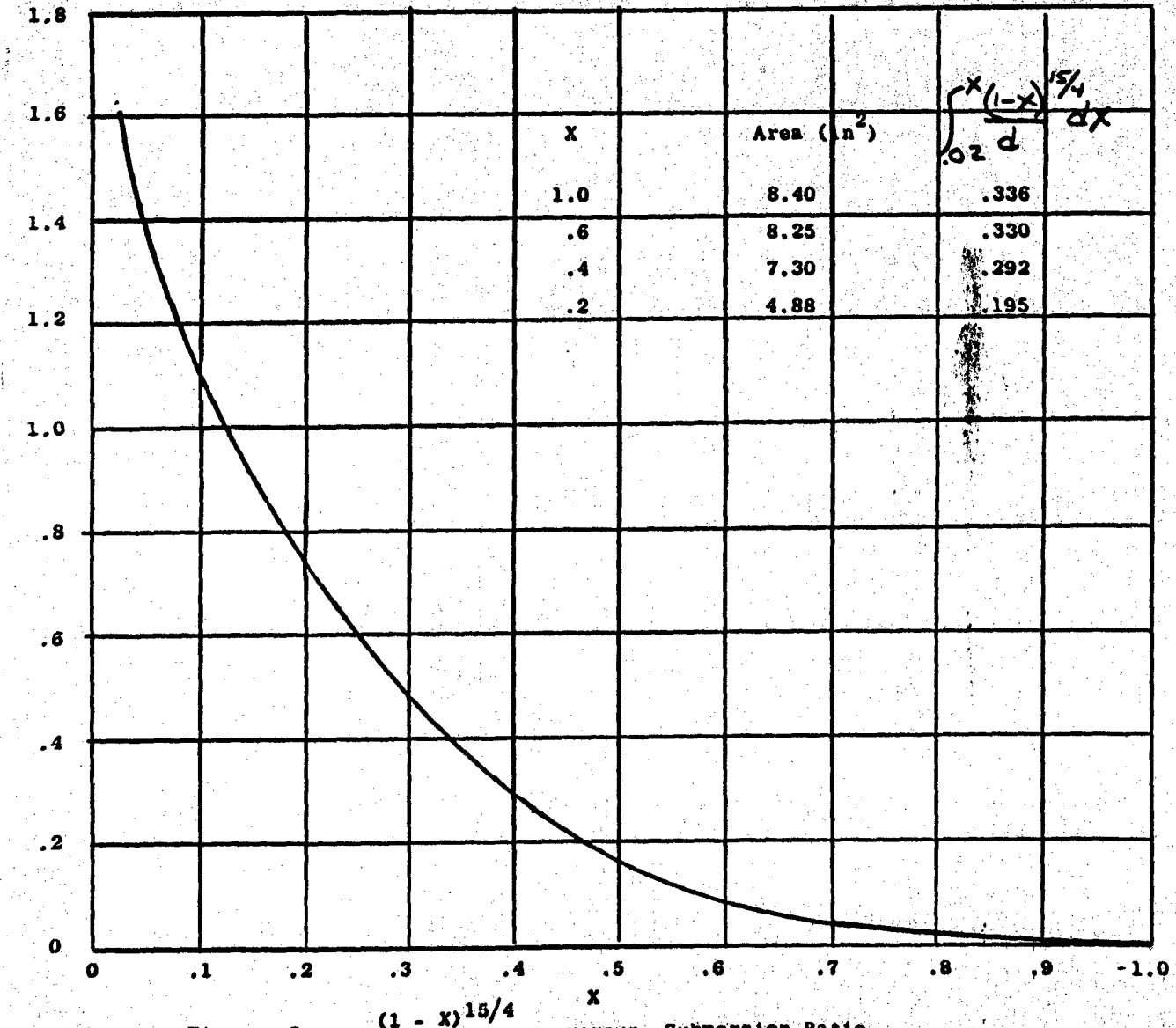

X	Area (in^2)	$\int_{.02}^{X} \frac{(1-x)^{15/4}}{d} dx$
1.0	8.40	.336
.6	8.25	.330
.4	7.30	.292
.2	4.88	.195

Figure 2 $\frac{(1 - X)^{15/4}}{d}$ versus Submersion Ratio

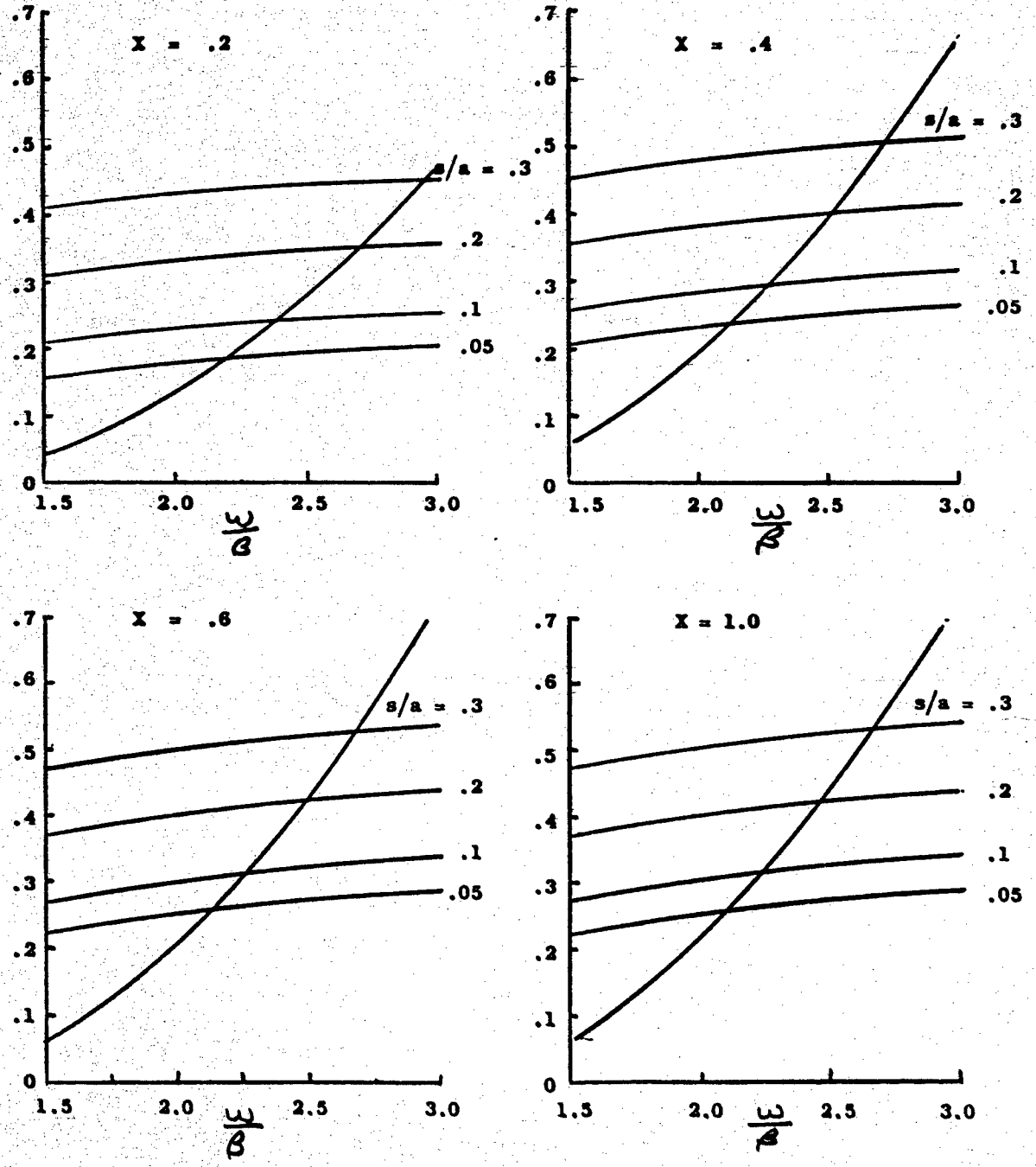

Determination of Velocity Ratios

Figure 3. Rotating Disk - Stationary Housing Seal

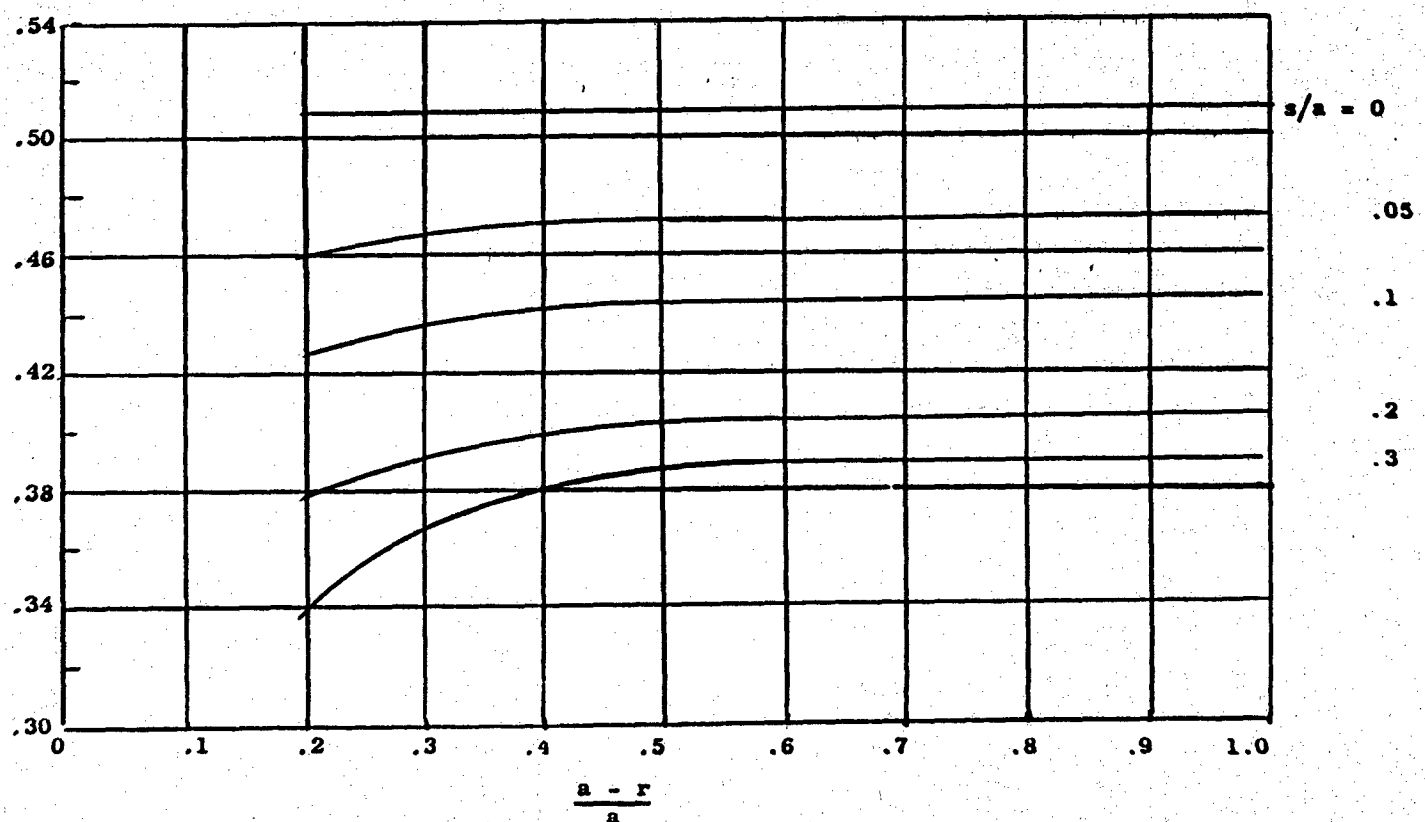

Velocity Ratio versus Submersion Ratio

Figure 4. Rotating Disk - Stationary Housing Seal

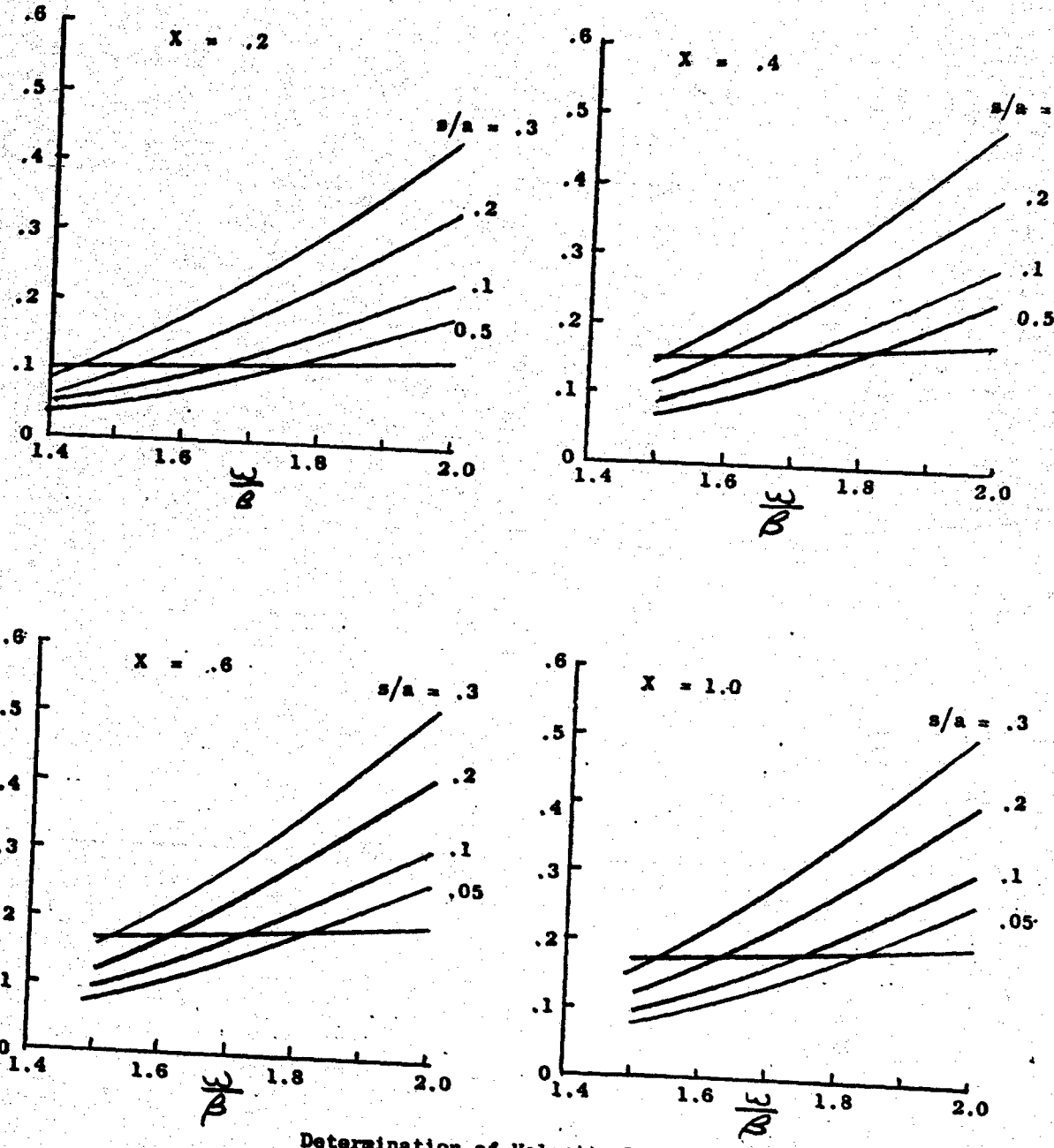

Determination of Velocity Ratios

Figure 5. Rotating Housing - Stationary Disk Seal

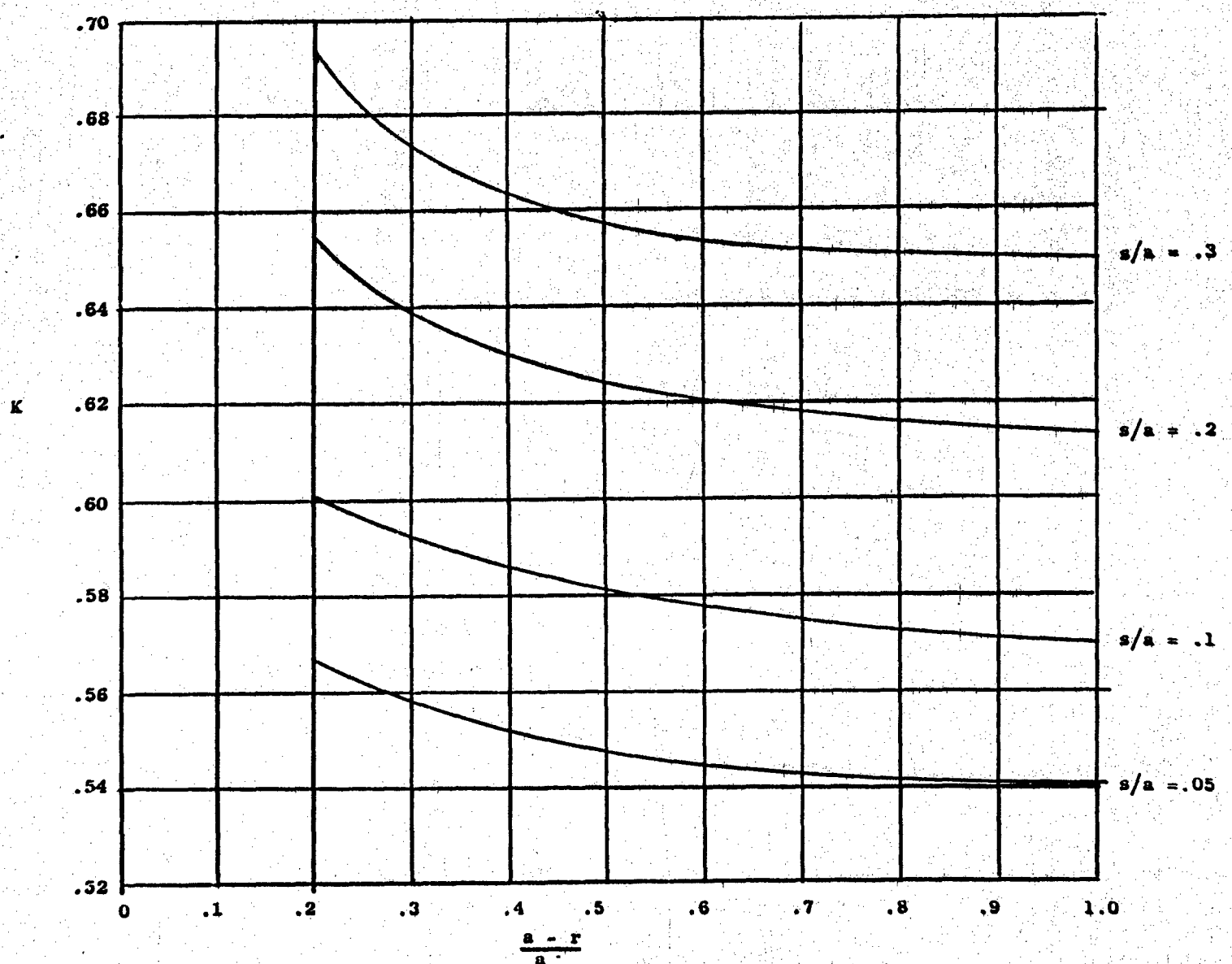

Figure 6. Rotating Housing - Stationary Disk Seal

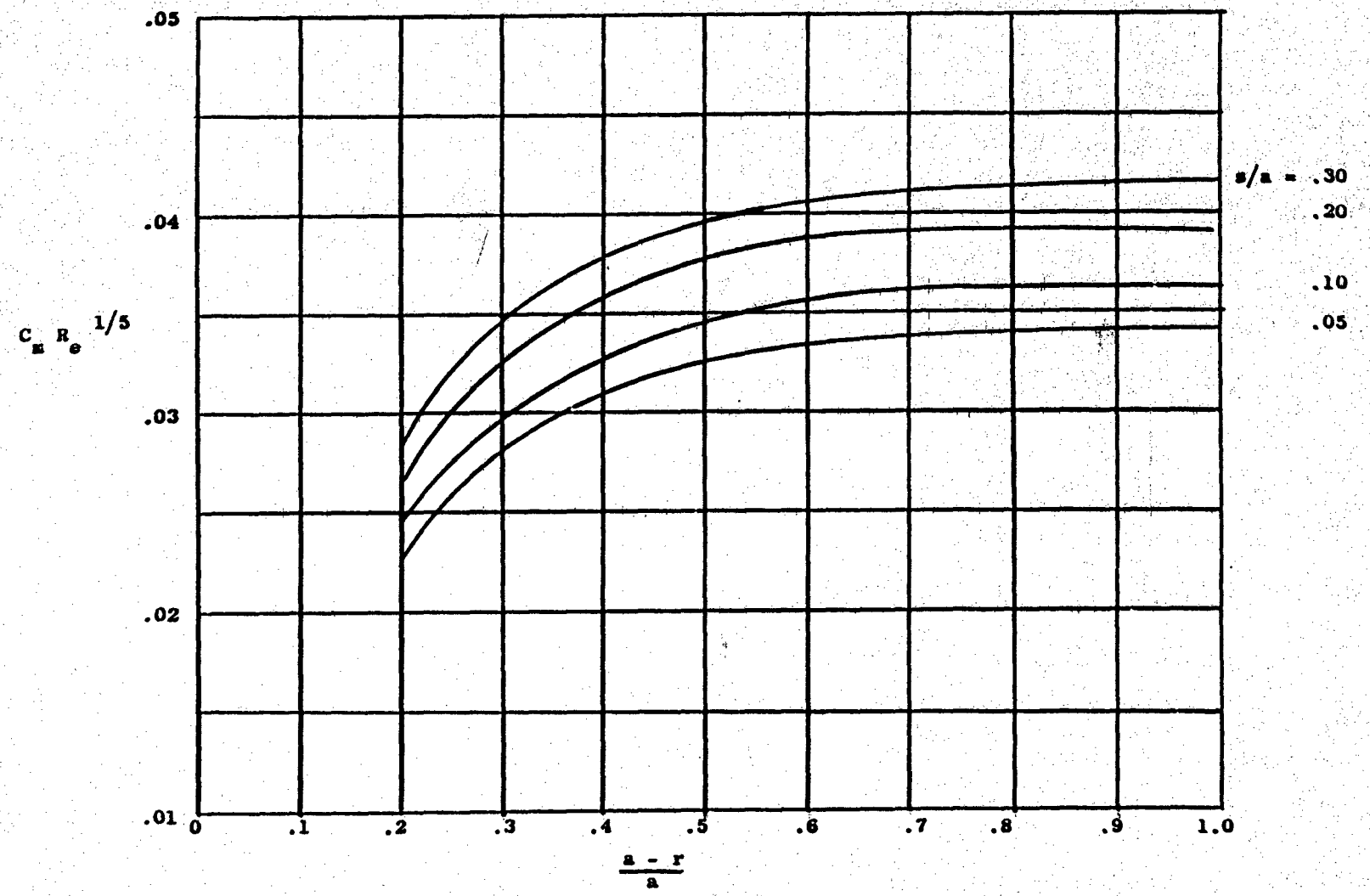

Torque Coefficient versus Submersion Ratio

Figure 7. Rotating Disk - Stationary Housing Seal

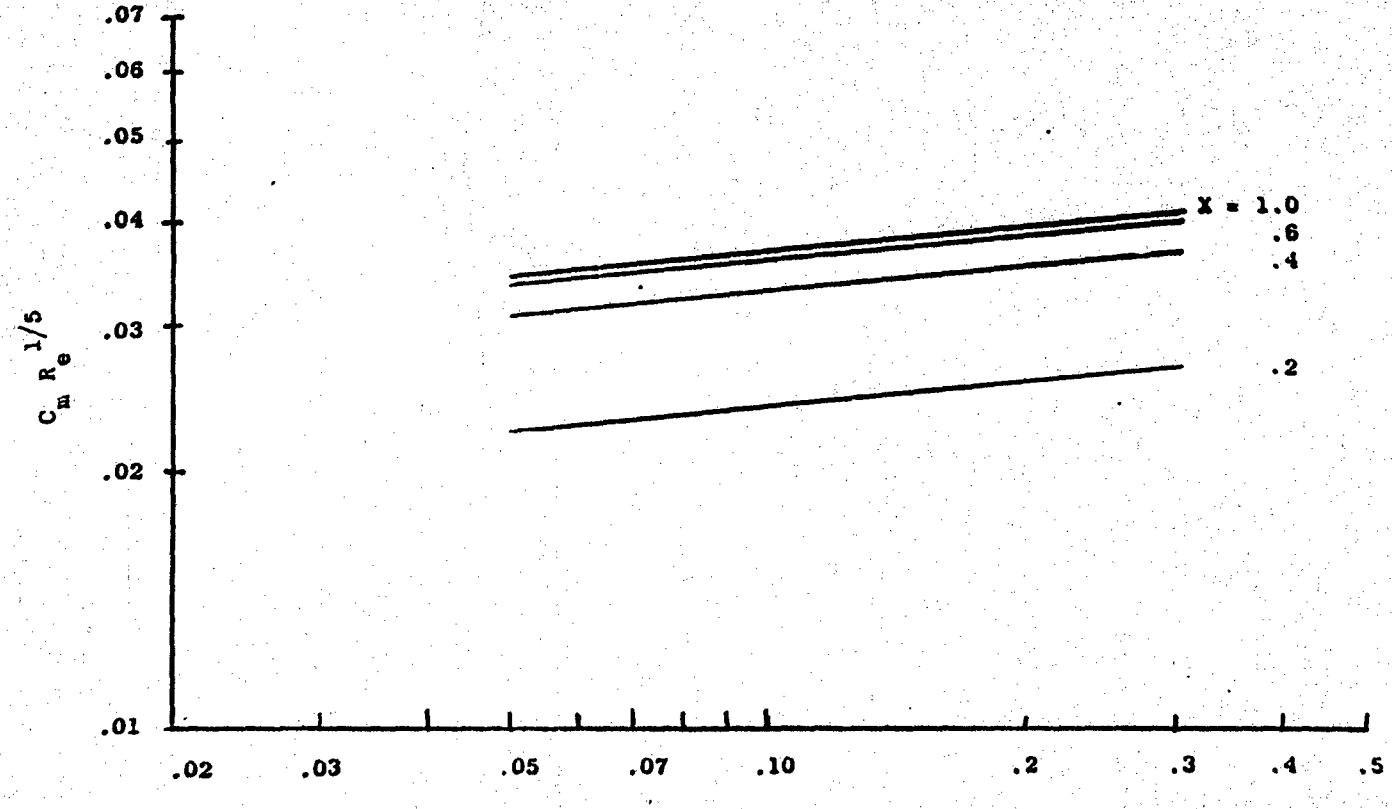

Figure 8. Rotating Disk - Stationary Housing Seal

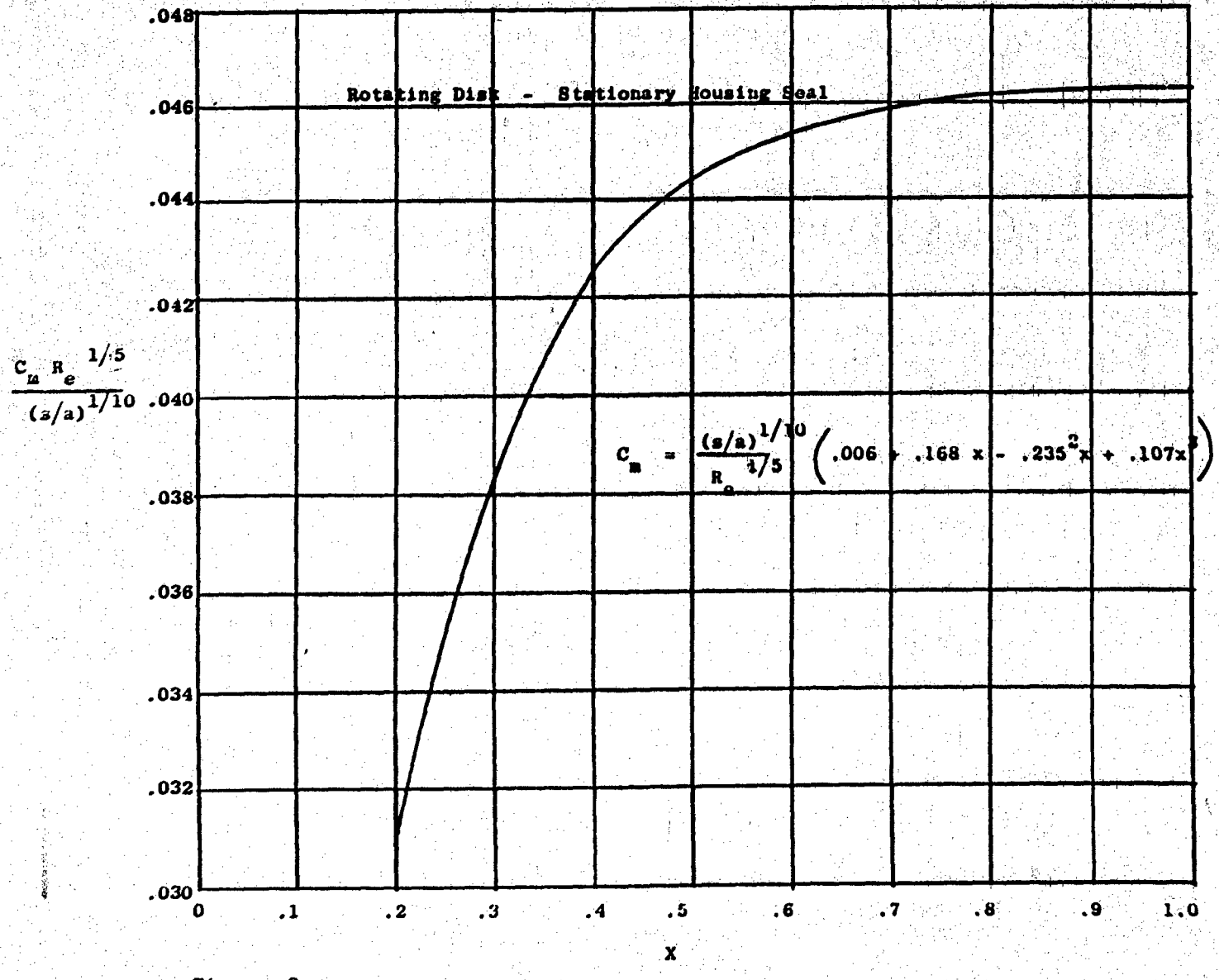
Rotating Disk - Stationary Housing Seal
$\frac{C_m R_e^{1/5}}{(s/a)^{1/10}}$
$C_m = \frac{(s/a)^{1/10}}{R_e^{1/5}} \left(.006 + .168\,x - .235\,x^2 + .107\,x^3\right)$
.048
.046
.044
.042
.040
.038
.036
.034
.032
.030
0
.1
.2
.3
.4
.5
.6
.7
.8
.9
1.0
X

Figure 9.

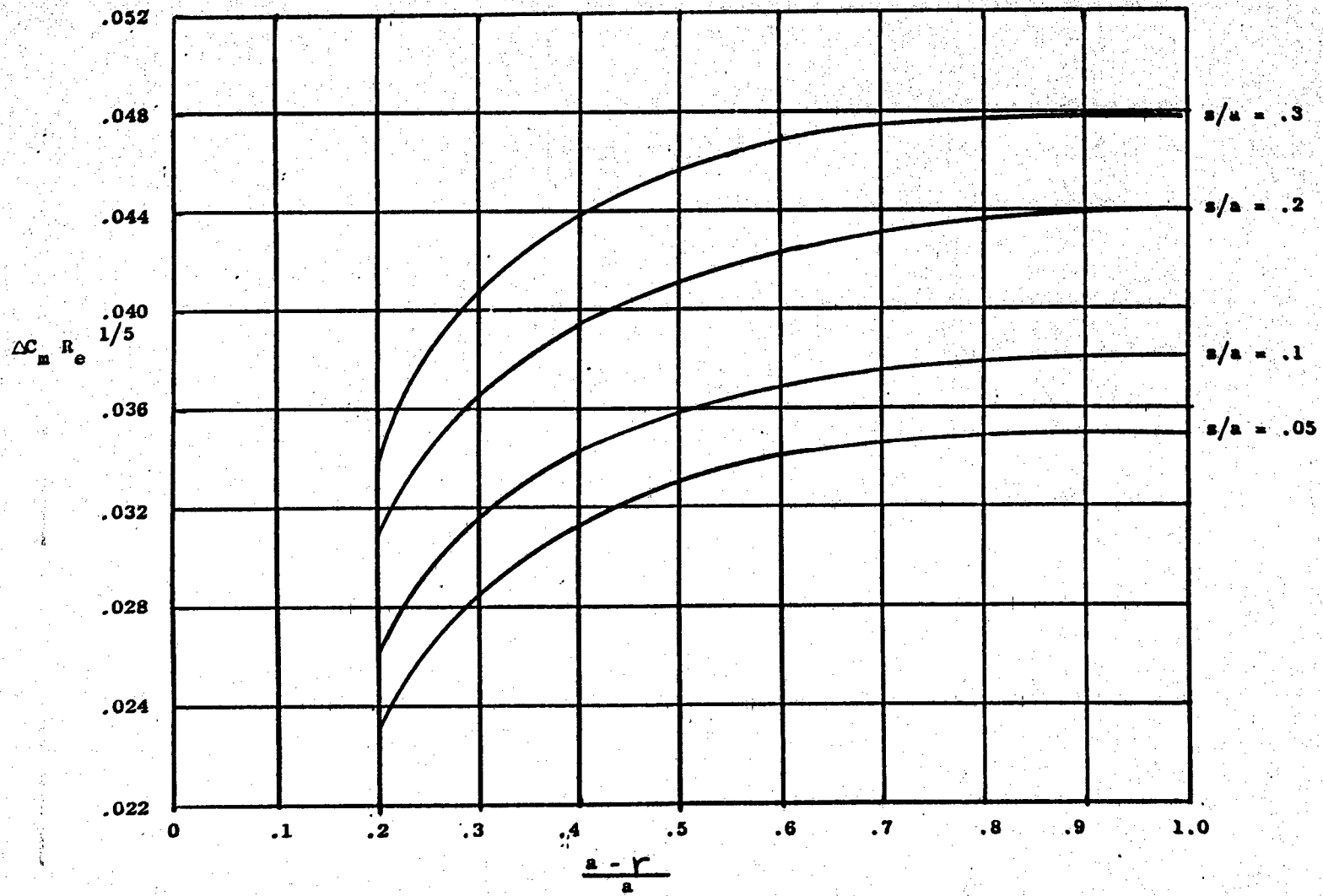

Torque Coefficient vs. Submersion Ratio

Figure 10. Rotating Housing Stationary Disk Seal

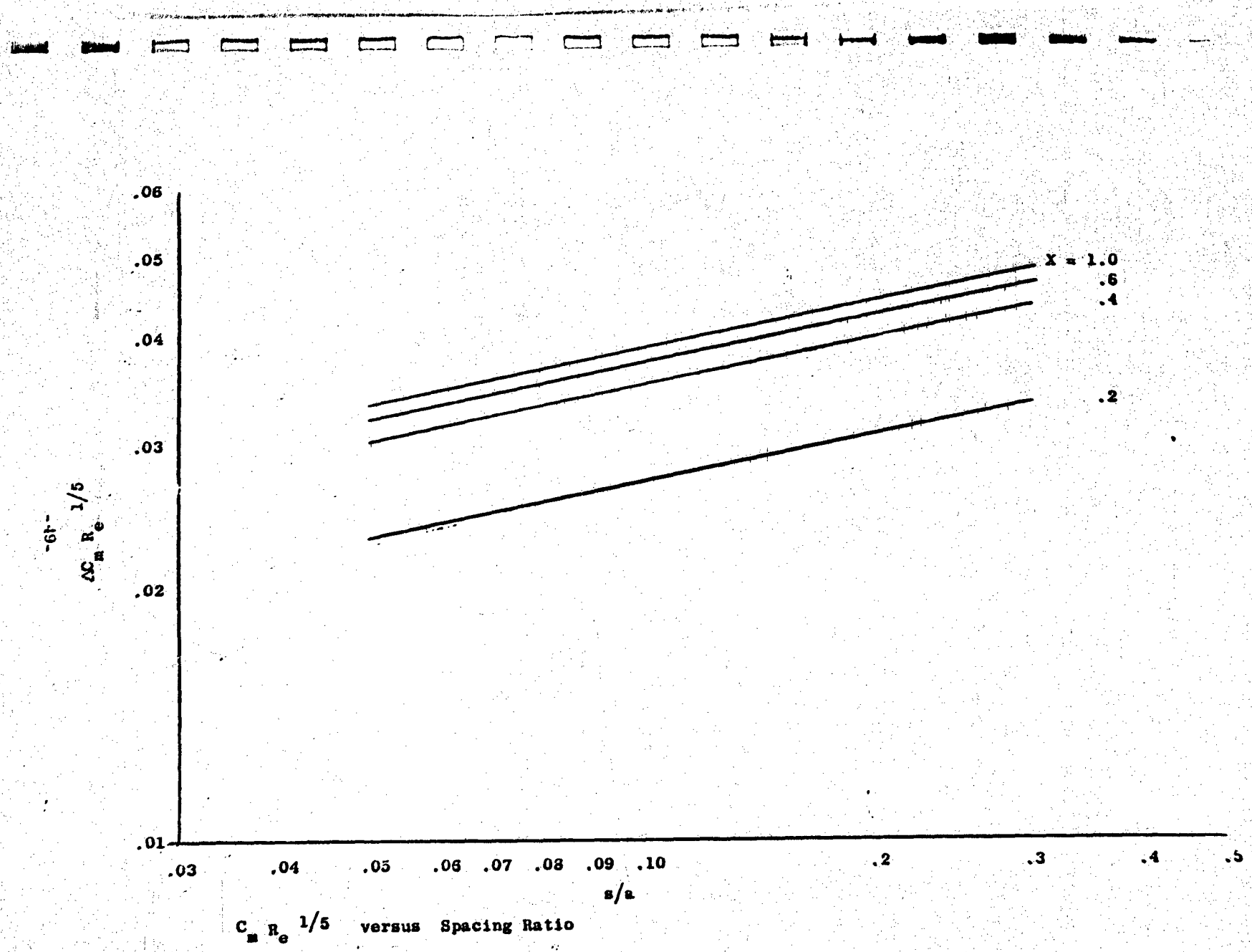

$C_m R_e^{1/5}$ versus Spacing Ratio

Figure 11. Rotating Housing - Stationary disk Seal

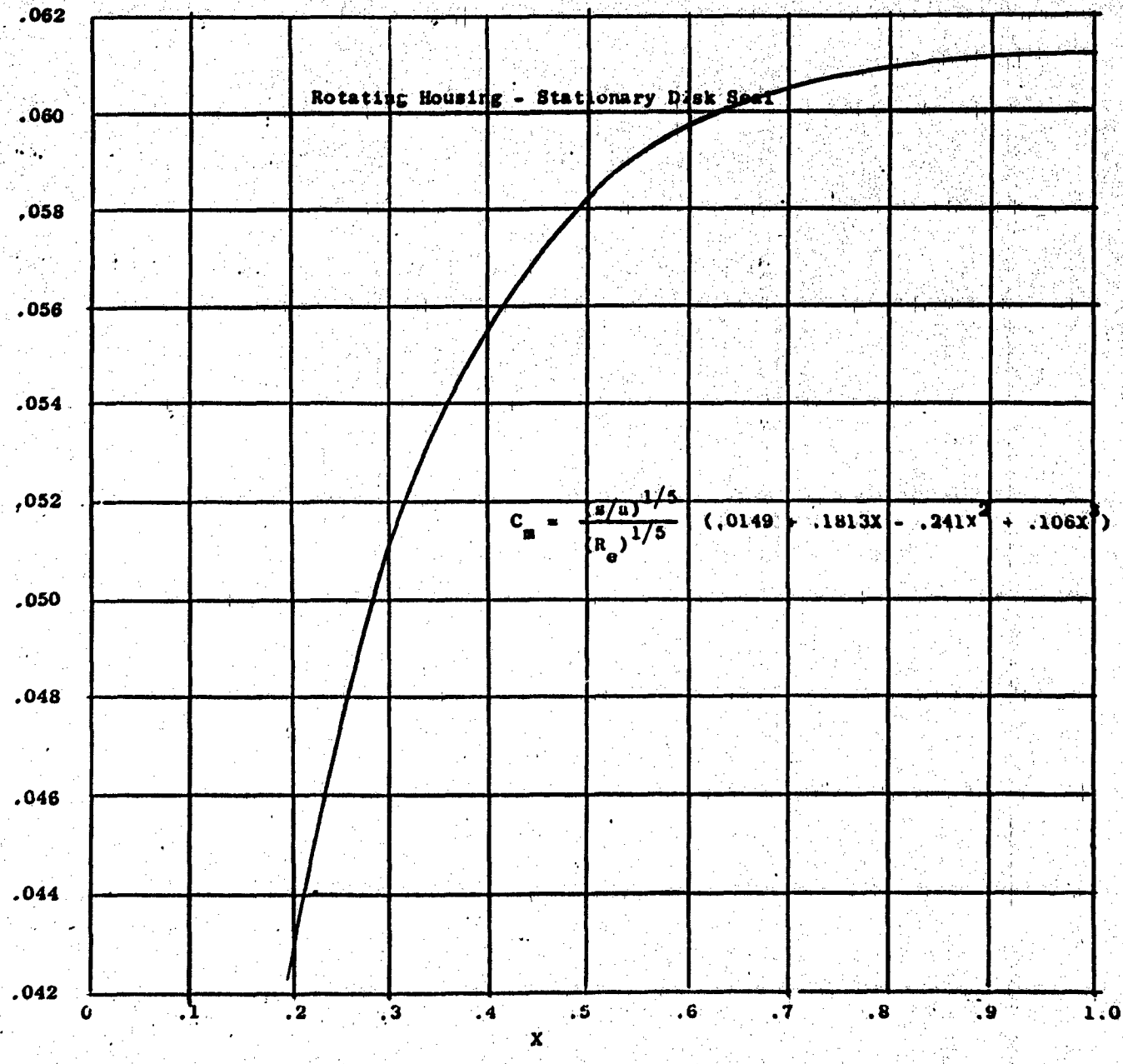
Rotating Housing - Stationary Disk Seal
$C_m = \frac{(s/a)^{1/5}}{(R_e)^{1/5}} (.0149 + .1813X - .241X^2 + .106X^3)$
$\frac{C_m R_e^{1/5}}{(s/a)^{1/5}}$
.062
.060
.058
.056
.054
.052
.050
.048
.046
.044
.042
0
.1
.2
.3
.4
.5
.6
.7
.8
.9
1.0
X

Figure 12.

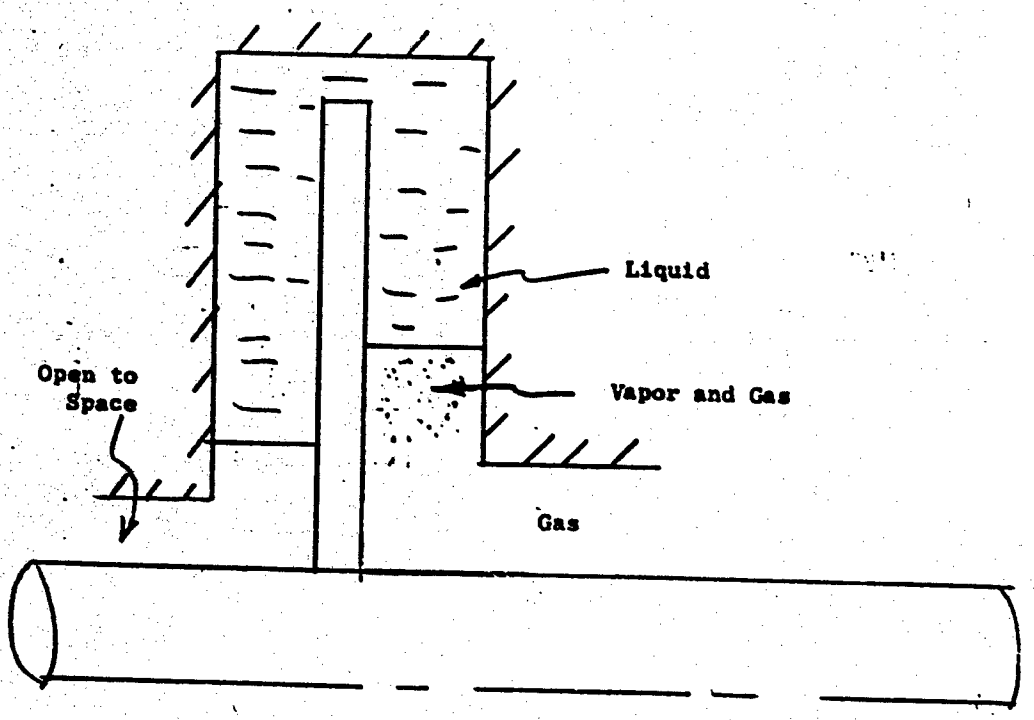

Figure 13. Rotating Disk Seal Schematic

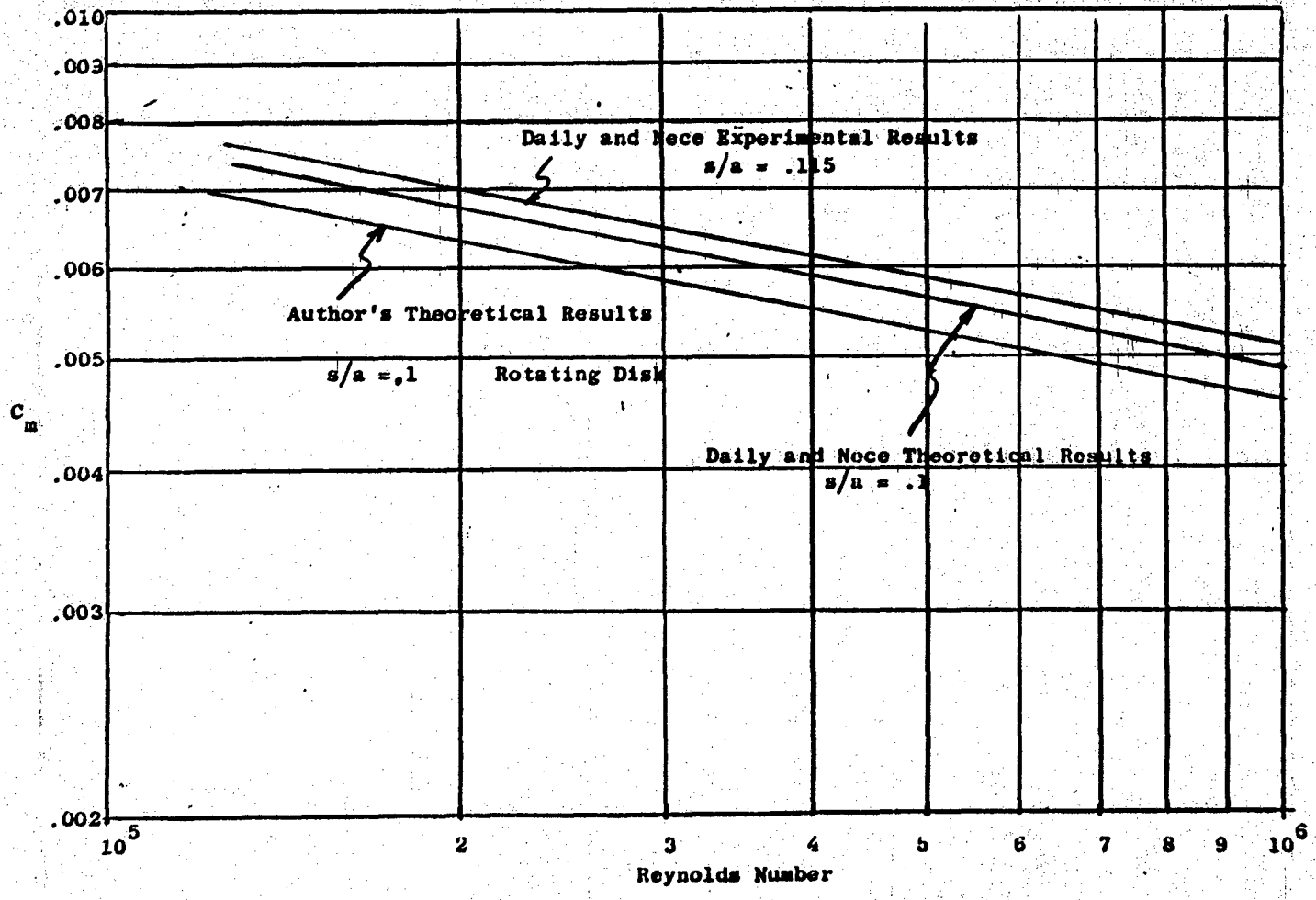

Figure 14. Comparison of Theoretical and Experimental Friction Coefficients

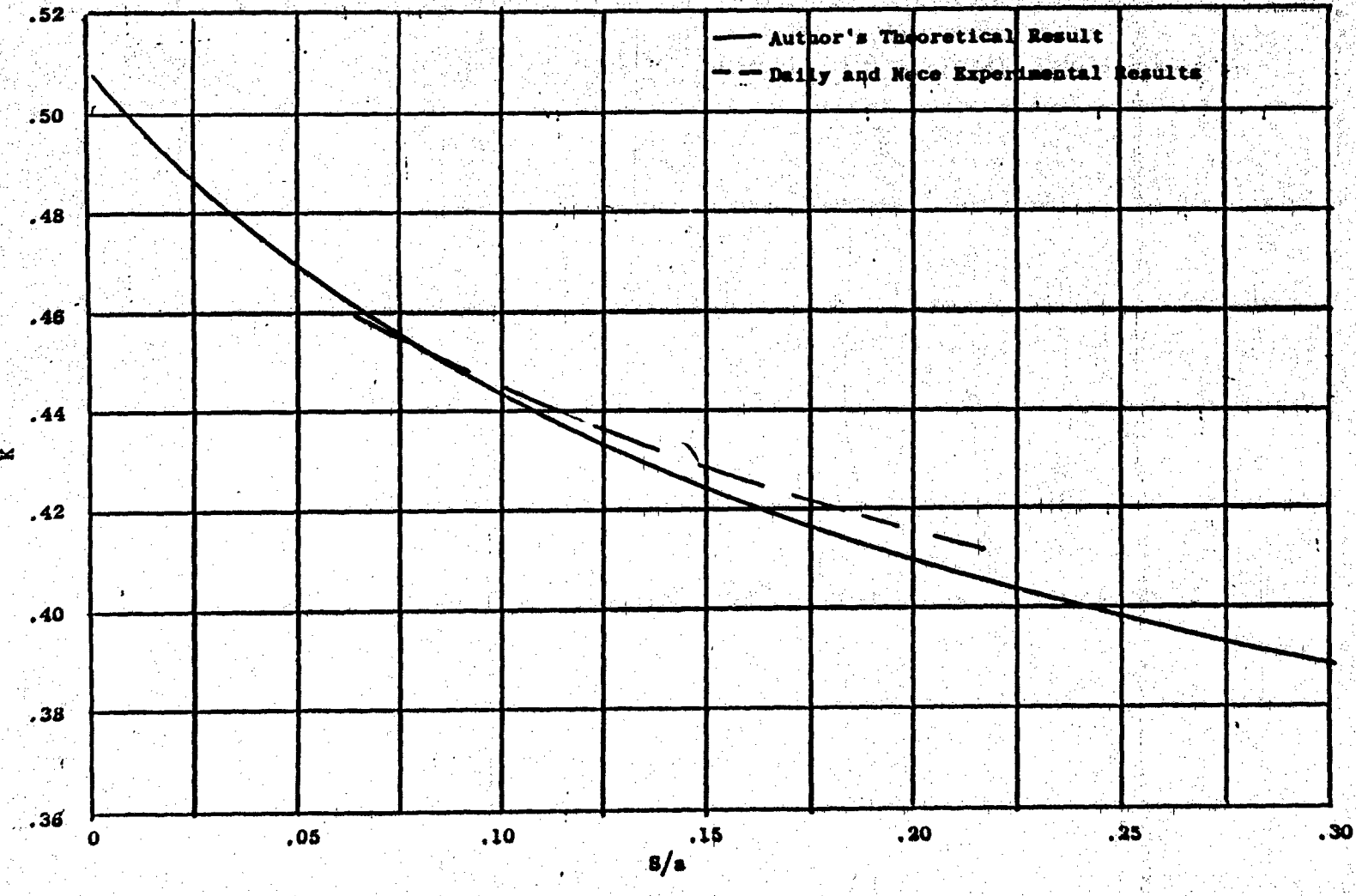

Figure 15. Comparison of Velocity Ratios for Fully Submerged Disks.

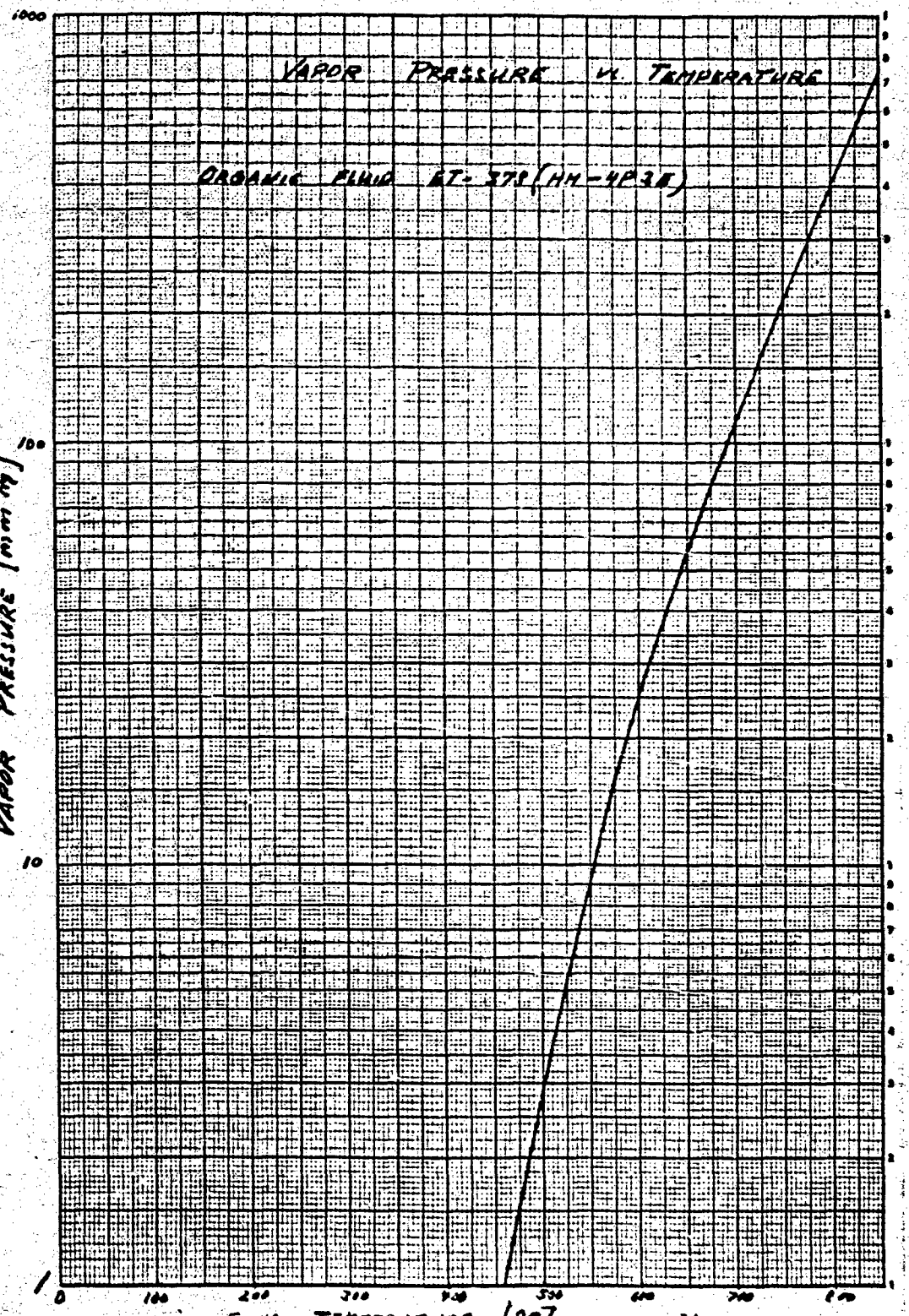
VAPOR PRESSURE vs. TEMPERATURE
ORGANIC FLUID RT-378 (HM-4P3E)
VAPOR PRESSURE [mm Hg]
1000
100
10
1
0
100
200
300
400
500
600
700
800
TEMPERATURE [°F]

Fig. 16

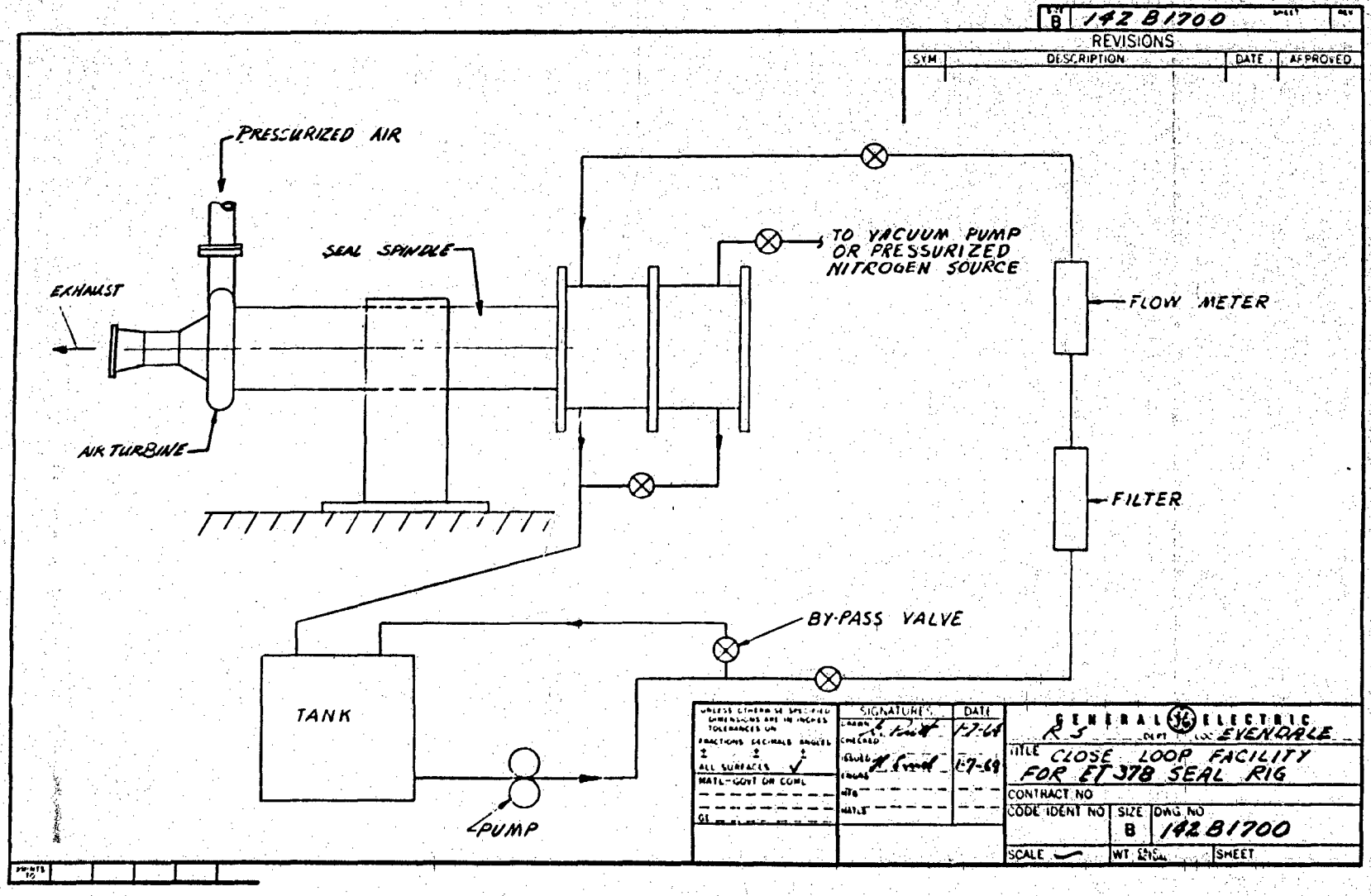
SIZE B 142B1700
REVISIONS
SYM
DESCRIPTION
DATE
APPROVED
PRESSURIZED AIR
SEAL SPINDLE
EXHAUST
AIR TURBINE
TO VACUUM PUMP OR PRESSURIZED NITROGEN SOURCE
FLOW METER
FILTER
BY-PASS VALVE
TANK
PUMP
SIGNATURES
DATE
GENERAL ELECTRIC
EVENDALE
TITLE CLOSE LOOP FACILITY FOR ET 378 SEAL RIG
CONTRACT NO
CODE IDENT NO
SIZE B
DWG NO 142B1700
SCALE
SHEET

Figure 17.

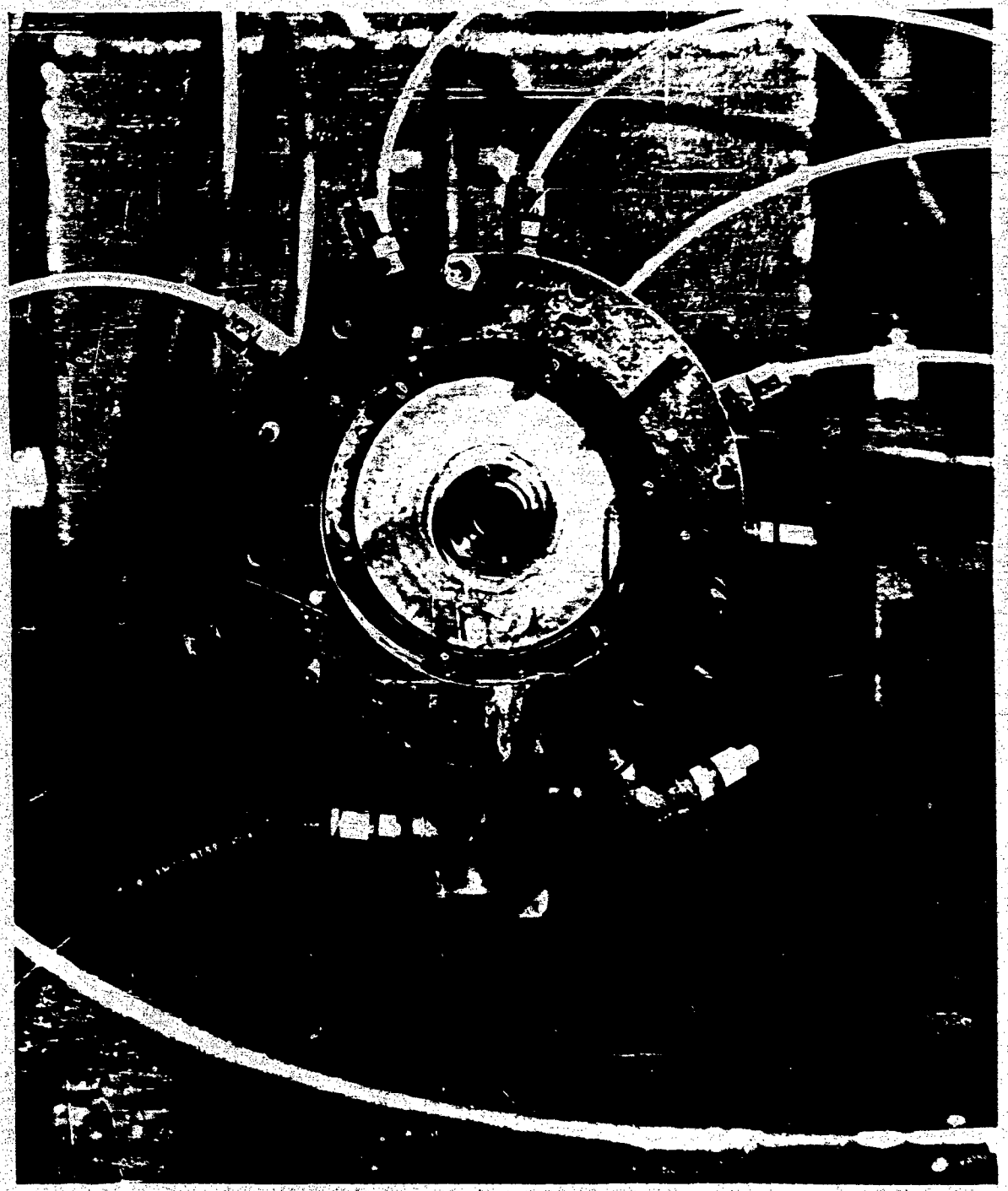

Figure 18. DZL - Seal (Narrow Axial Gap Configuration) Operating at 9900 RPM in Normal Air Atmosphere. ET 378 Fluid is Used As Sealing Fluid.

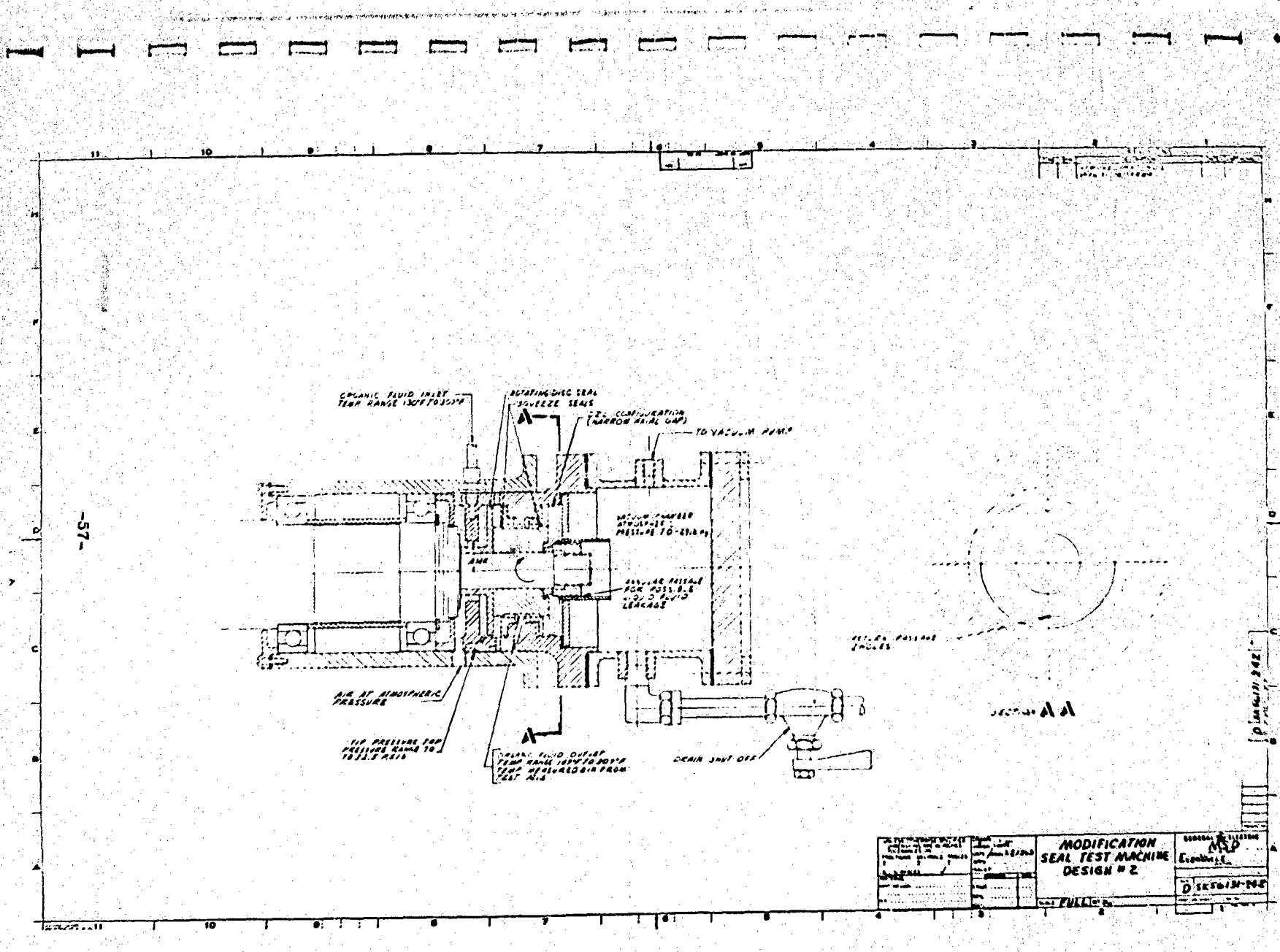
ORGANIC FLUID INLET
TO VACUUM PUMP
AIR AT ATMOSPHERIC PRESSURE
DRAIN SHUT OFF
MODIFICATION
SEAL TEST MACHINE
DESIGN # 2

Figure 19.

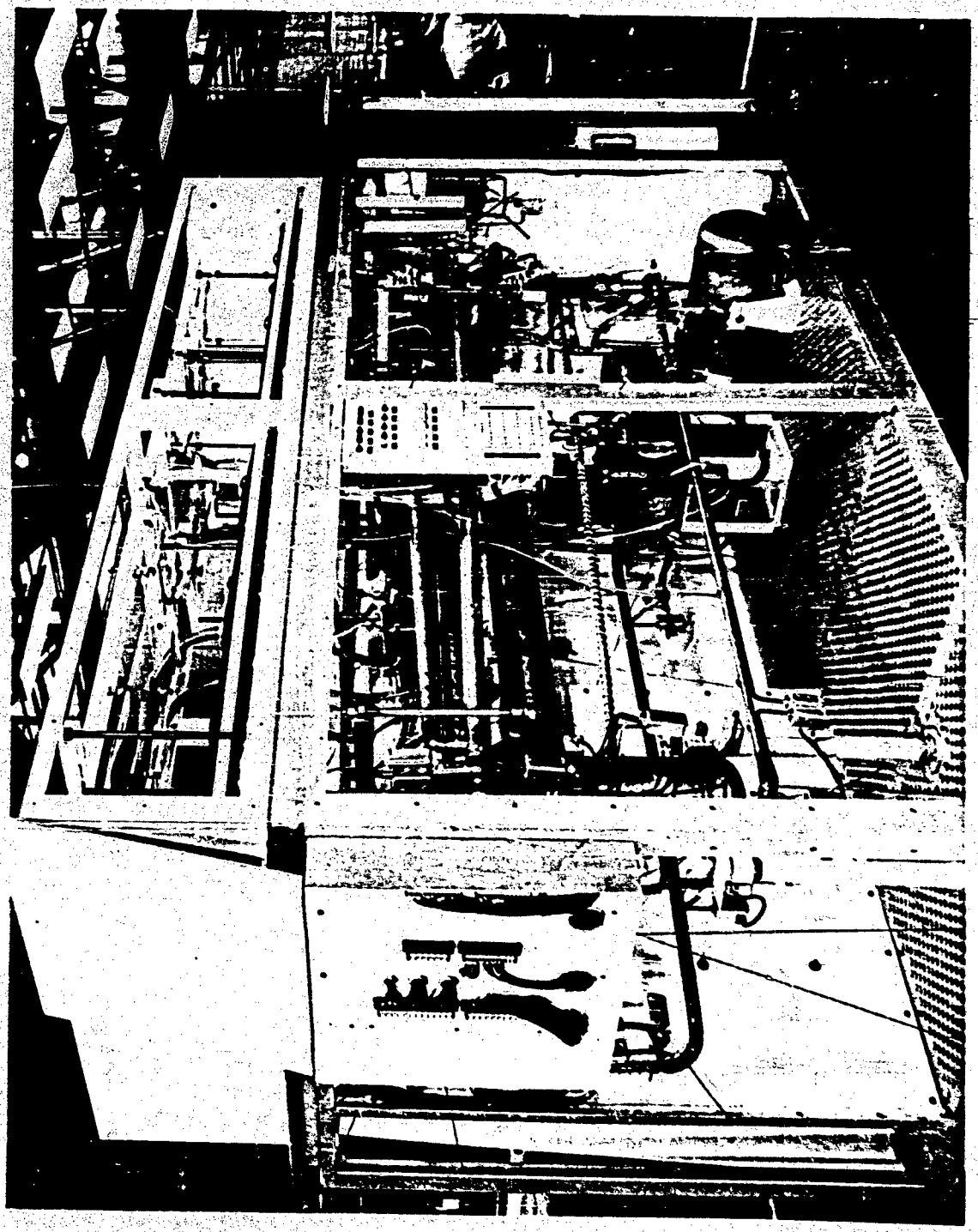

Figure 20. Liquid Metal Seal Test Console.

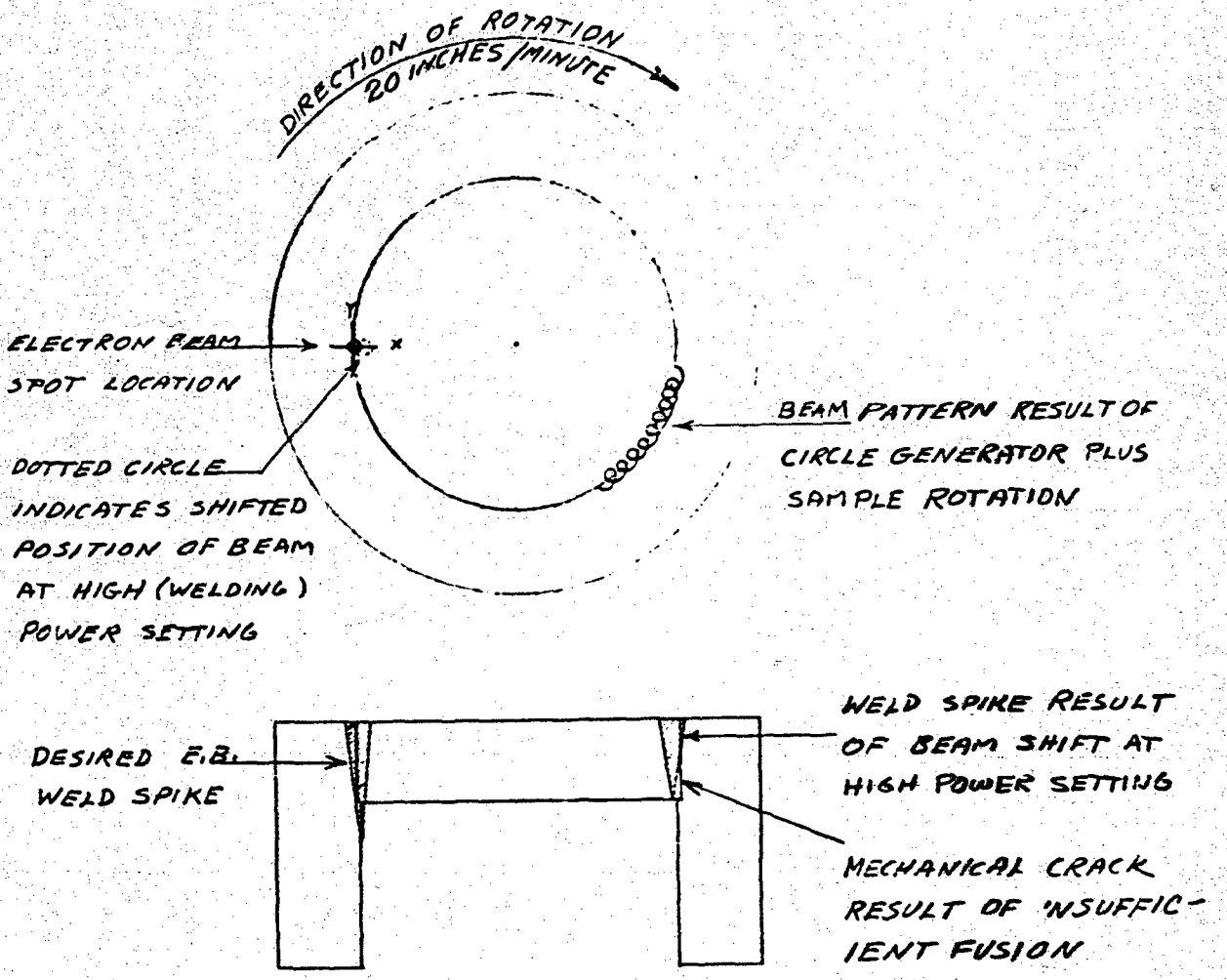
DIRECTION OF ROTATION
20 INCHES/MINUTE
ELECTRON BEAM
SPOT LOCATION
DOTTED CIRCLE
INDICATES SHIFTED
POSITION OF BEAM
AT HIGH (WELDING)
POWER SETTING
BEAM PATTERN RESULT OF
CIRCLE GENERATOR PLUS
SAMPLE ROTATION
DESIRED E.B.
WELD SPIKE
WELD SPIKE RESULT
OF BEAM SHIFT AT
HIGH POWER SETTING
MECHANICAL CRACK
RESULT OF INSUFFIC-
IENT FUSION

Figure 21

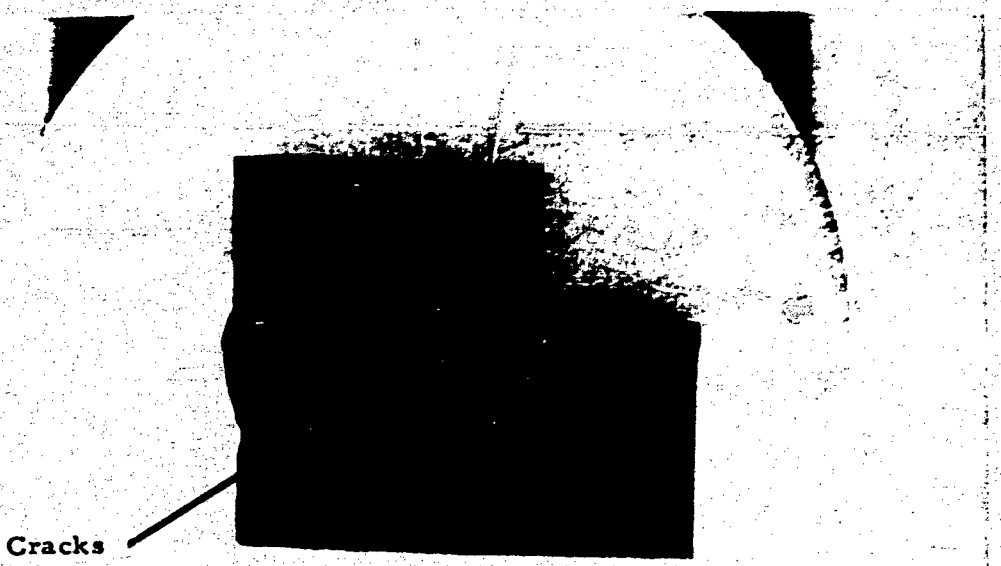

Figure 22.

SPECIMEN A:

CONDITION: Spherodized Anneal

HISTORY:
1) Pre-heated Approximately 800°F
2) Electron Beam Welded
3) Tempered
4) Annealed
5) Hardened and Tempered

REMARKS: Minute Cracks Discovered During Metallographic Examination. Cracks Loacted in Weld Metal-Base Metal Boundary Near Point of Spike.

C63091319

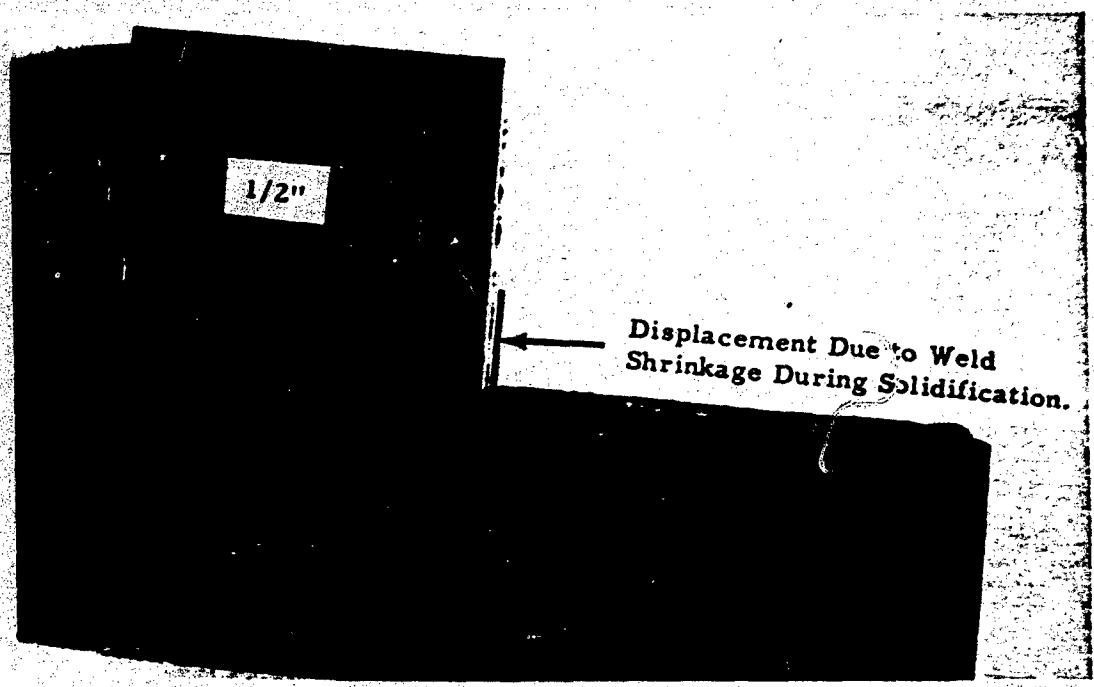

Figure 23.

SPECIMEN B:

CONDITION: Sperodized Anneal

HISTORY:
1) Pre-heat Approximately 800°F
2) Electron Beam Welded
3) Cracked
4) Tempered
5) Repair Welded
6) Cracked

REMARKS: Weld Crack Propogated from Notch Created by Incomplete Fusion of Joint.

CG3091318

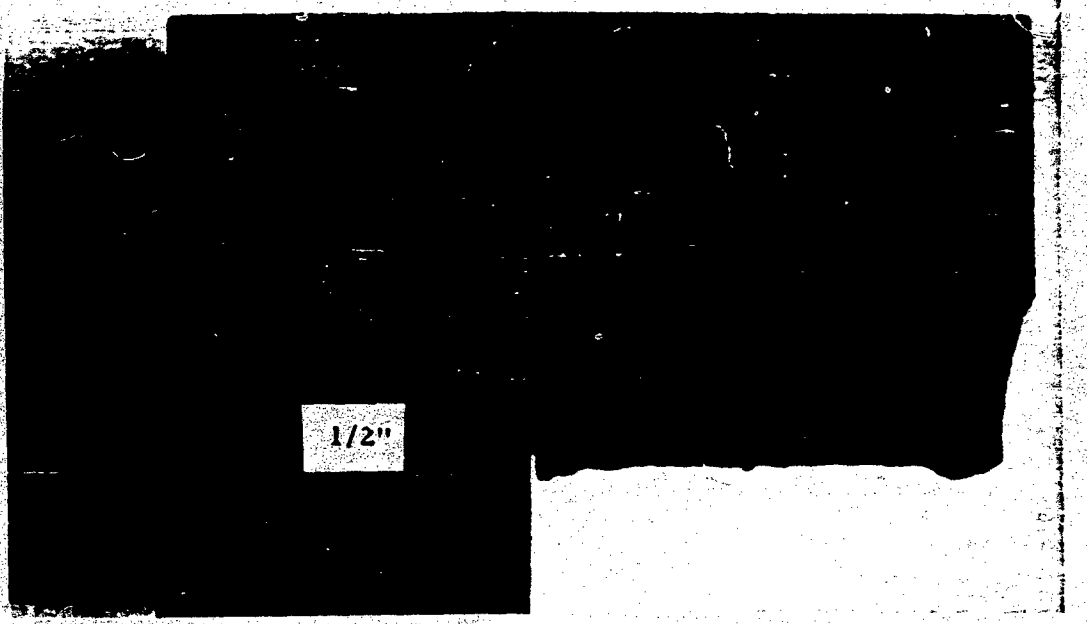

Figure 24.

SPECIMEN B:

CONDITION: Spherodized Anneal

HISTORY:
1) Pre-heat Approximately 800°F
2) Electron Beam Welded
3) Cracked
4) Tempered
5) Repair Welded
6) Cracked (See Figure 3)

REMARKS: This section shown 180° from Figure 2 is not Cracked Because of Complete Fustion of Joint and Stress Relief Accomplished when Weaker Portion of Sample Cracked.

C83091317

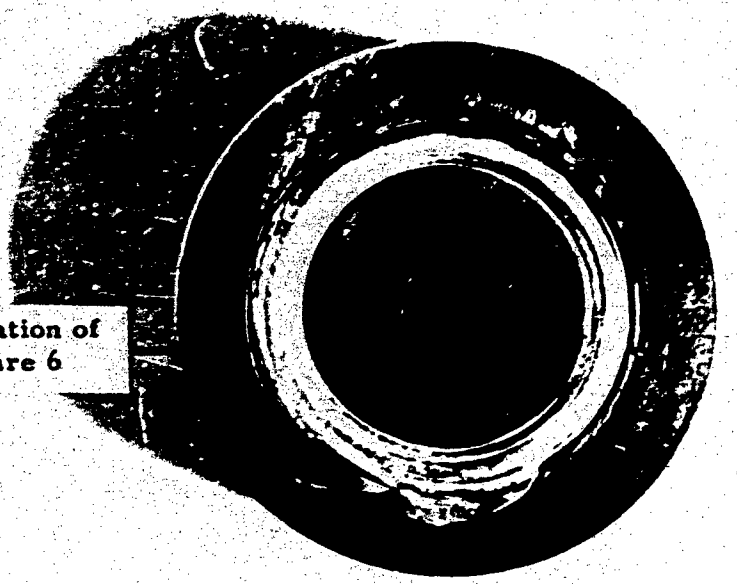

Figure 25.

SPECIMEN D:

CONDITION: Hardened, Tempered at 1650°F

HISTORY:
1) Pre-heat Approximately 800°F
2) Electron Beam Welded
3) Cracked and Lifted

REMARKS: The Electron Beam Shifted Radially Inward During Welding Resulting in this Defective Weldment. The "Knitting" Trace of the Electron Beam can be Seen on this Weld Bead.

C63091316

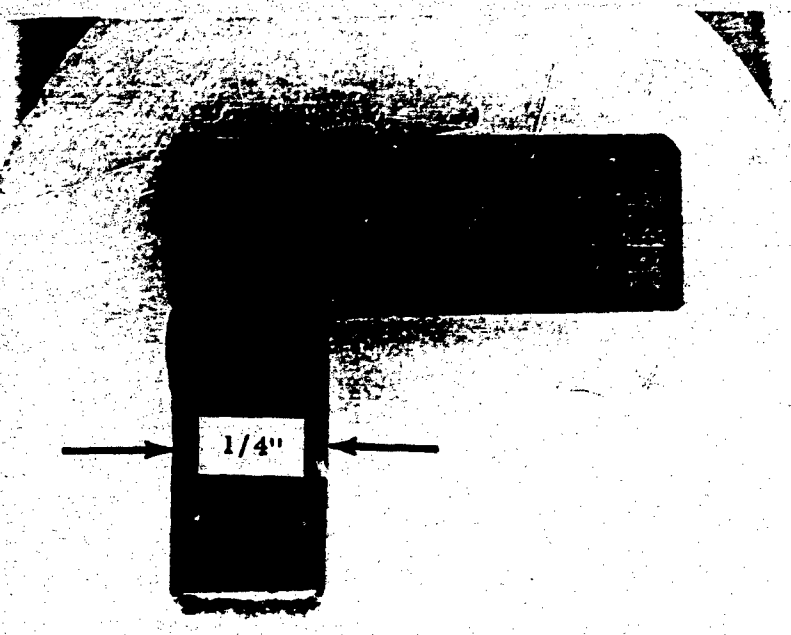

Figure 26.

SPECIMEN D:

CONDITION: Hardened, Tempered at 1650°F

HISTORY:
1) Pre-heat Approximately 800°F
2) Electron Beam Welded
3) Cracked and Lifted (See Figure 5)

REMARKS: Cross Section of Weld Indicating Location of Weld Spike.

C33091315

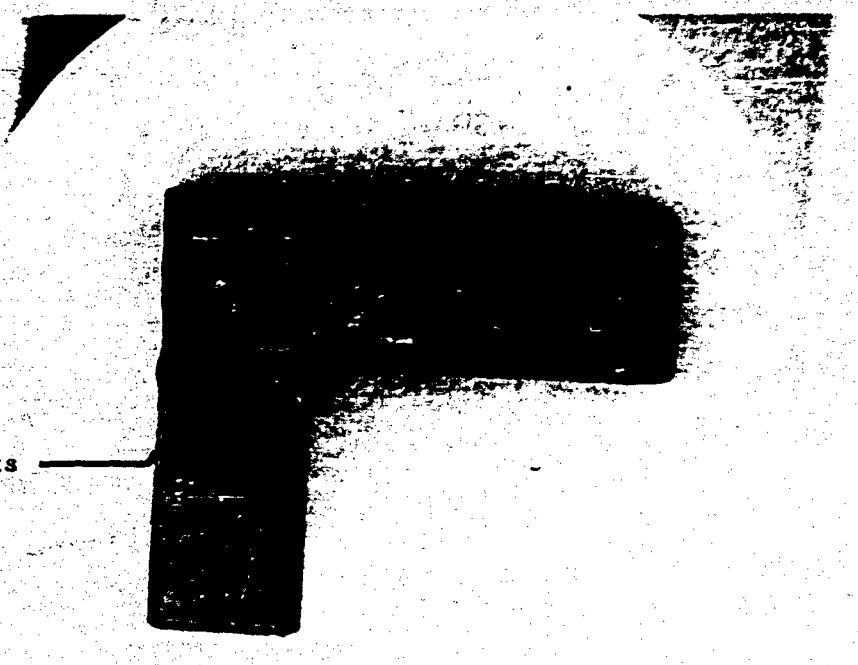

Figure 27.

SPECIMEN E:

CONDITION: Hardened, Tempered at 1450°F

HISTORY:
1) Pre-heat at Approximately 800°F
2) Electron Beam Welded
3) Immediately Tempered

REMARKS: Cursory Inspection after Welding Disclosed No Cracks; Assembly was Therefore Tempered and Sectioned for Metallography. Metallographic Examination Disclosed Cracks in the Center of the Weld Spike.

C33091314

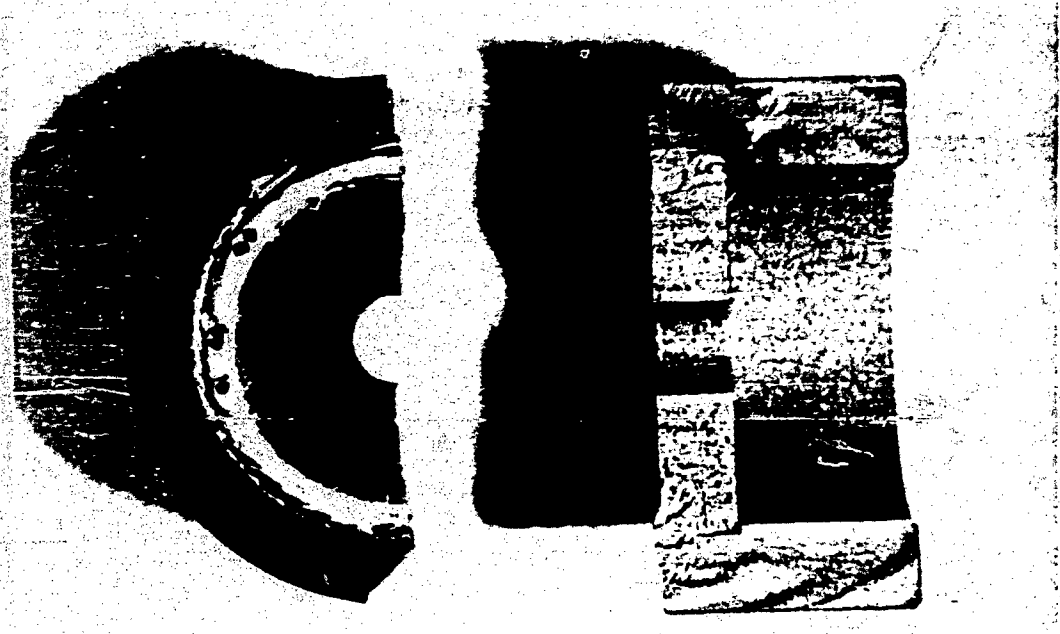

Figure 28.

SPECIMEN F:

CONDITION: Hardened, Tempered at 1250°F

HISTORY:
1) Pre-heat at Approximately 800°F
2) Electron Beam Welded
3) Cracked

REMARKS: This Specimen Appeared to have been Successfully Welded; Upon Removal from the Electron Welding Machine and While Being Examined, the Specimen Burst Apart Accompanied by a Gun-Like Report.

C53091313

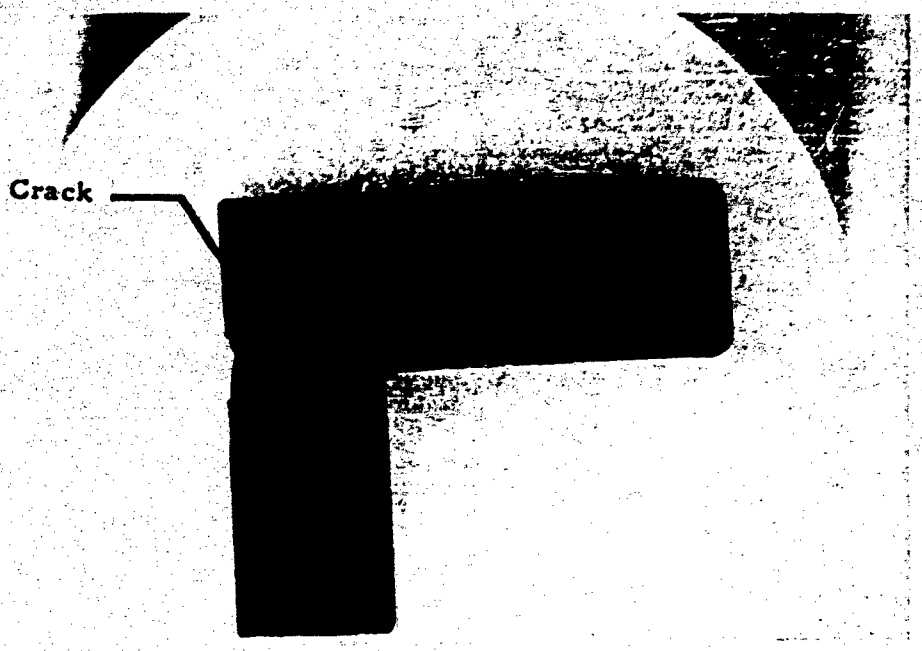

Figure 29.

SPECIMEN F:

CONDITION: Hardened, Tempered at 1250°F

HISTORY:
1) Pre-heat at Approximately 800°F
2) Electron Beam Welded
3) Cracked

REMARKS: Cross Section of Burst Specimen Showing Location of Crack and the Shift of the Weld Spike. Penetration was Good and Spike well Formed.

C63091312

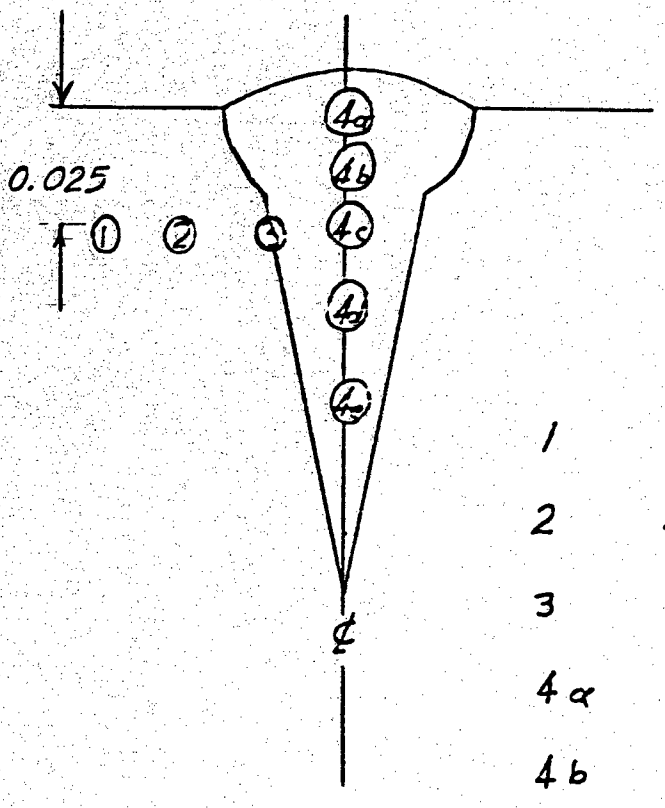

1	R_c 56.5
2	R_c 58
3	R_c 61
4a	R_c 63
4b	R_c 62
4c	R_c 61.5
4d	R_c 62
4e	R_c 60.5

Figure 30. Hardness Survey of Electron Beam Weld in Hardened and Tempered Rex 49.

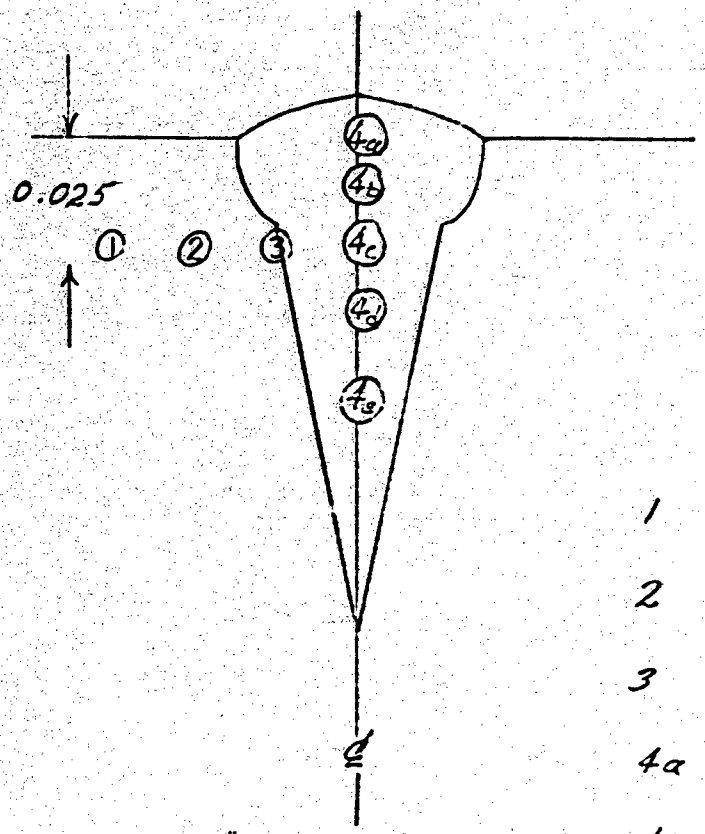

1 Rc 28.5

2 Rc 43

3 Rc 55.5

4a Rc 62

4b Rc 60

4c Rc 61

4d Rc 62

4e Rc 57.5

Figure 31. Hardness Survey of Electron Beam Weld Annealed Rex 49.

REFERENCES

1. Daily, J., and Nece, R., "Chamber Dimension Effects on Induced Flow and Frictional Resistance of Enclosed Rotating Disks," ASME Paper No. 59- Hyd-9.

2. Schlichting, H., "Boundary Layer Theory," McGraw-Hill Book Company.

3. Ernst, H., "Liquid Metal Bearings and Seals, Volume II - Seals."

4. Brocker, E., "Theorie and Experiment Zum Reibungswiderstand der Glatten Rotierenden Scheibe Bei Turbulenter Stroemung," Zeitschrift fur Angewandte Mathematik and Mechanik Bd 39, Nr 112, 1959.

5. Schultz - Grunow, F., "Der Reibungswiderstand rotierender Scheiben in Gehausen," Zeitschrift fur Angewandte Mathematik und Mechanik, Band 15, Heft 4, July, 1935.

6. Bird, R., Stewart, W., and Lightfoot, E., "Transport Phenomena", John Wiley and Sons, 1960.

DISTRIBUTION LIST

Copies	Organization
1	ASD (ASRCNL-2, Mr. John Morris) Wright Patterson AFB, Ohio
1	ASD (ASNPPS-3, Mr. R. Ling) Wright Patterson AFB, Ohio
1	ASD (ASRCNL, Mr. G. A. Beane) Wright Patterson AFB, Ohio
2	ASD (ASRMFP-3, Mr. R. J. Smith) Wright Patterson AFB, Ohio
1	U. S. Atomic Energy Commission Office of Technical Information P. O. Box 62 Oak Ridge, Tennessee
1	Thompson Ramo Wooldridge Attn: Mr. Carl Nau 23555 Euclid Avenue Cleveland 17, Ohio
1	Rocketdyne Division North American Aviation Attn: Mr. R. B. Dillaway Department 584 6633 Canoga Park Boulevard Canoga Park, California
1	Technical Information Center Aerospace Corporation P. O. Box 95085 Los Angeles 45, California
10	ASTIA Arlington Hall Station Arlington 12, Virginia

1	Cleveland Graphite Bronze Division of Clevite Corporation Attn: Mr. E. James Vargo 17000 St. Clair Avenue Cleveland 10, Ohio
1	SSD (SSTRE, Capt. W. W. Hoover) AF Unit Post Office Los Angeles 45, California
1	Power Information Center Moore School Building 200 South 33rd Street Philadelphia 4, Pennsylvania
1	National Aeronautics and Space Administration Lewis Research Center Attn: Mr. Joseph Joyce Space Electric Power Office 25000 Brookpark Road Cleveland 35, Ohio
1	AiResearch Manufacturing Company Attn: Mr. John Dennan 402 - 536th Street Phoenix 34, Arizona
1	Sundstrand Aviation Corporation Attn: Mr. K. Nichols 2480 West 70 Denver 21, Colorado
1	Aerojet-General Nucleonics Attn: Mr. Paul Wood Azusa, California
1	Pratt & Whitney Aircraft Division of United Aircraft Corp. Attn: Mr. Frederick A. Corwin East Hartford, Connecticut

1	Mechanical Technology Inc., Attn: Mr. F. K. Orcutt Albany-Shaker Road Latham, New York
1	Ion Physics Corporation Attn: Dr. A. Stuart Denholm P. O. Box 98 Burlington, Mass.
1	Mr. G. G. Thur NASA-Lewis Research Center 21000 Brookpark Road Cleveland 35, Ohio